Structure formation in the universe: comparison of some observations and models

T. Padmanabhan

Theoretical Astrophysics Group, Tata Institute of Fundamental Research, Homi Bhabha Road, Bombay 400 005, India
Present address: Inter-University Centre for Astronomy and Astrophysics, Post Bag 4, Ganeshkhind, Pune 411 007, India

Recent cosmological observations like the detection of large scale streaming motion, APM and QDOT surveys, detection of temperature anisotropy in the microwave background radiation (MBR) etc., impose severe constraints on models for structure formation. The theoretical background for these models and the restrictions arising from the observations are reviewed. In particular, the COBE satellite results for the temperature fluctuation $(\Delta T/T)_{rms}=(1.1\pm0.2)\times10^{-5}$ and $(\Delta T/T)_Q=(0.48\pm0.15)\times10^{-5}$ are consistent with a scale-invariant spectrum, of density perturbations $\sigma(R)=(R_0/R)^2$ at large scales with $R_0\simeq(23.9\pm2.1)\,h^{-1}$ Mpc. This is consistent with APM data and large scale streaming velocity measurements (both of which require $\sigma\,(50\,h^{-1}\,\text{Mpc})\simeq0.2$) provided the scale-invariant spectrum is extrapolated from $3000\,h^{-1}$ Mpc to $50\,h^{-1}$ Mpc. Comparing the shape of $\sigma(R)$ at $R\lesssim60\,h^{-1}$ Mpc, determined from galaxy surveys (IRAS, CfA, and APM), with the COBE result, we find that a relatively rapid bend in $\sigma(R)$ around $R\approx(40-60)\,h^{-1}$ Mpc is needed. The fact that COBE results match with galaxy survey results at $50\,h^{-1}$ Mpc suggests that biasing is not significant at $R\gtrsim50\,h^{-1}$ Mpc. On the other hand a CDM spectrum, normalized to the COBE value, will overshoot galaxy survey results at small scales. Such a spectrum can be consistent with observations only if the biasing varies with scale and $b<1$ at small scales. The implications of this result are discussed.

1. Introduction and scope

OBSERVATIONS suggest that our universe is homogeneous and expanding at scales larger than about $100\,h^{-1}$ Mpc. At smaller scales, however, there exist several kinds of inhomogeneities in the form of galaxies, clusters and superclusters. It seems reasonable to model such a universe along the following lines: We assume that the universe was smoother in the past but contained small density inhomogeneities. The gravitational attraction of overdense regions will then make the density inhomogeneities grow, thereby eventually producing the structures we see today. Several variations on this theme are possible and have indeed been tried out in the literature. It is probably fair to say that: (i) There is considerable evidence supporting the basic idea that structures have formed through gravitational instability; but, (ii) we do not have today any comprehensive model for structure formation which does not run into serious difficulties with regard to some observation or the other.

One of the reasons for this—rather dichotomous—situation is that observational data relevant to structure formation have improved tremendously in recent years. There exist sufficient data to guide model building and theoretical speculation and there is sufficient scope—in the near future—to test reasonable predictions from the theories. This review attempts to highlight this interplay between some of the crucial observations and models for structure formation. I have tried to present the observations in a unified manner so that maximum amount of information can be extracted from them. Since all simple models have failed to explain the observations adequately, it is probably best at this stage to try to identify the essential features of a future model which has a reasonable chance for explaining the observations. Such an attempt will clearly be phenomenological; but it is indeed gratifying that the currently available data allow such an attempt to be carried out to its completion.

In order to keep the review to a reasonable length, I had to limit its scope in several ways. To begin with, I have avoided all detailed derivations, whenever such material is available elsewhere (a detailed discussion of many of these topics can be found in references 1, 2). I have also not attempted to discuss the technical details and statistical significance of observations except when they are crucial to argument. The growth of perturbations in the nonlinear regime is discussed at a more

detailed level than is usual in such a review. This is done because I feel that this area has not been explored in the literature to the extent it should have been.

2. Theoretical background

Models for structure formation which are based on the concept of gravitational instability contain three basic ingredients in their make up: a background Friedmann model describing the smooth universe; a mechanism for generating the initial perturbations in this universe and, finally, a mechanism for amplifying these seed perturbations. We begin by summarizing each of these ingredients.

2.1 *The background Friedmann model*

The background model can be characterized by a number of parameters, which, for our purpose, may be taken to be the following.

(i) The expansion rate is determined by the Hubble constant at the present epoch, $H_0 \equiv H(t_0) \equiv (\dot{a}/a)_0 \equiv 100\,h$ km s^{-1}, where $a(t)$ is the expansion factor and $t = t_0$ is the present moment. Observations suggest that $0.5 \leq h \leq 1.0$.

(ii) The energy density is specified using a density parameter, Ω, defined to be $\Omega = [\rho(t_0)/\rho_c]$, where $\rho(t_0)$ is the *total* energy density today and $\rho_c = (3H_0^2/8\pi G) = 1.88 \times 10^{-29} h^2$ gcm^{-3}. Observations[3] suggest that $0.2 < \Omega < 3$. We shall make the choice of $\Omega = 1$ when the result does *not* crucially depend on this assumption; when it does, we shall be careful to indicate the Ω dependence. There are several *theoretical* reasons to favour the value of $\Omega = 1$ though there is no compelling observational reason for this choice. This choice, however, makes the mathematical analysis quite simple in several cases.

(iii) We also need to specify the composition of matter in the universe today. For our purposes, it is sufficient to specify the individual density parameters for the radiation (Ω_R), vacuum-energy (Ω_{vac}), baryons (Ω_B) and nonbaryonic dark matter (Ω_{DM}). The radiation density includes contribution from all the particles which are relativistic today (photons, massless fermions, etc.) and are governed by the equation of state $p_R = (1/3)\rho_R$. The vacuum density is contributed by any component which has the equation-of-state $p_{vac} = -\rho_{vac}$; in particular, a cosmological constant will fall in this class. The baryons and nonbaryonic dark matter can be treated as pressure-free dust with the equation of state $p_B = p_{DM} = 0$. Obviously, we must have $\Omega = \Omega_R + \Omega_{vac} + \Omega_B + \Omega_{DM}$. Observations[3,4] suggest that: (a) the photon contribution Ω_γ to Ω_R is $\Omega_\gamma = 2.56 \times 10^{-5} h^{-2}$; (b) $0.011 \leq \Omega_B h^2 \leq 0.037$; and (c) $\Omega_{DM} > 0.2$. There is very little handle on the value of Ω_{vac}. The bounds (b) and (c) together imply that the dark matter must have a nonbaryonic component. For concreteness, we shall assume that the dark matter (at least, part of it) is made of elementary, weakly interacting, neutral fermions of mass m.

Given these parameters one can construct a background Friedmann model. As an example, consider a model with $\Omega_{DM} \gg \Omega_B$ (say, $\Omega_{DM} \simeq 0.9$, $\Omega_B \simeq 0.1$), $\Omega_{vac} = 0$ and $\Omega_R = \Omega_\gamma$. The evolution of such a model will proceed along the following lines: During the very early phases of the evolution, the universe will be radiation-dominated with $a(t) \propto t^{1/2}$. A transition to a matter-dominated phase will occur at the redshift of $z \simeq z_{eq}$, where $(1 + z_{eq}) = (\Omega_{DM}/\Omega_R) \simeq 3.9 \times 10^4\, \Omega h^2$. (For $t > t_{eq}$, the form of $a(t)$ depends on the value of Ω. If $\Omega = 1$, then $a(t) \propto t^{2/3}$; this is a good approximation for $z \gtrsim 100$ in all models.) Notice that, since $\Omega_{DM} \gg \Omega_B$, the dominant energy density at $z \lesssim z_{eq}$ is due to *dark matter* and not due to baryons. The baryons and the electrons will be strongly coupled to the photons at this epoch. Somewhat later in the evolution, at $z \simeq z_{dec}$ with $z_{dec} \simeq 1100$, the electrons and nuclei will combine together to form neutral atoms of hydrogen and helium. The photons will decouple from matter at this epoch and will propagate thereafter with negligible scattering. The structures like galaxies etc. will form significantly later at $z \ll z_{dec}$.

The evolution can be different if Ω_{vac} is significant. As a second example, consider a universe with $h = 0.7$, $\Omega = 1$, $\Omega_B = 0.03$, $\Omega_{DM} = 0.17$ and $\Omega_{vac} = 0.8$. In such a model, $(\rho_{DM}/\rho_{vac}) = 0.25(1+z)^3$ so that for $z \lesssim z_{vac} \simeq 0.59$ the vacuum energy ('cosmological constant') dominates over matter. For $z \ll z_{eq} \simeq 2300$, the expansion factor will evolve as $a(t) = (\Omega_{DM}/\Omega_{vac})^{1/3} \sinh^{2/3}(3\sqrt{\Omega_{vac}}\, H_0\, t/2)$. The 'age' of such a universe will be larger than a model with $\Omega = 1$, $\Omega_{vac} = 0$ at all redshifts. (For example, $t_0 = 1.1\, H_0^{-1}$ for this model compared to $0.667\, H_0^{-1}$ for the $\Omega_{vac} = 0$ model.) Such models can, sometimes, help to overcome the difficulties in more conventional models.

2.2 *The origin of perturbations*

All models for structure formation assume that there existed small perturbations around the Friedmann model in the very early universe. The detailed evolution of the models depend, to some extent, on the nature of

these perturbations and how they originate.

In general, one can characterize a mildly inhomogeneous universe by specifying a density distribution function of the form $\rho(t,\mathbf{x})=\bar{\rho}(t)\,[1+\delta(t,\mathbf{x})]$, where $\delta \ll 1$. It is more convenient, however, to work with $\delta_{\mathbf{k}}(t)$ which is the Fourier transform of $\delta(\mathbf{x},t)$. (If the background universe has $\Omega \neq 1$, then it is more appropriate to use some other complete set of functions rather than plane waves. This complication does not affect the conclusions which we are interested in.) It will then be possible to study the evolution of the density perturbation $\delta_{\mathbf{k}}(t)$ by some suitable approximation schemes. However, notice that a function like $\rho(t,\mathbf{x})$ or $\delta_{\mathbf{k}}(t)$ contains far more information than we require, in the sense that it specifies the actual density at any spacetime event. What we are actually interested in will be the *statistical* properties of the density distribution in some large region of the universe. For this purpose, it is usual to assume that any given (large) region of the universe constitutes a realization out of an ensemble of possible density distributions. In this case, there will exist a probability functional $\mathscr{P}[\delta_{\mathbf{k}},t]$ specifying the probability that the density contrast is described by the Fourier coeffieients $\delta_{\mathbf{k}}$ at any given time t. This probability functional will contain the full statistical information about the density contrast.

Any model which produces the initial density contrast should also specify the statistical properties of the density contrast by giving this probability functional $\mathscr{P}[\delta_k,t]$. Two separate physical mechanisms have been explored in the literature for the possible origin of the initial density perturbation. The first one[5] uses quantum fluctuations in the very early universe to generate classical density perturbations at some later epoch. These models usually lead to a probability functional $\mathscr{P}$ which is a guassian. In this case, all the statistical information about the density perturbation is contained in the two-point-function $P(k)=\langle|\delta_k|^2\rangle$ which is called the power spectrum of the fluctuation. The second class of models[6] use some suitable form of seeds arising in the early universe, to produce the perturbations. These seeds (like strings, textures, primordial black holes, etc.) accrete matter around them by gravitational attraction and thus produce inhomogeneities in the density distribution. The statistical characterization of such a perturbation is much more complicated; in general it will not be guassian. The power spectrum $P(k)=\langle|\delta_k|^2\rangle$ is well-defined even in this case though it does not completely characterize the probability distribution. In the linear regime, however, $P(k)$ is the most important statistic in all models.

The power spectrum determines several other physically relevant quantities. Consider, for example, the mean-square-fluctuation $\sigma^2(R)=\langle(\delta M/M)_R^2\rangle$ in the mass contrast within a sphere of radius R placed somewhere in the universe. It is easy to show that

$$\sigma^2(R)=\int_0^\infty \frac{dk}{k}\left(\frac{k^3\,P(k)}{2\pi^2}\right)\left[\frac{3(\sin kR-kR\cos KR}{(kR)^3}\right]^2 \quad (1)$$

Clearly, each logarithmic interval in k contributes an amount $\Delta^2(k)\equiv(k^3\,P(k)/2\pi^2)$ to the mass fluctuation at a scale $R\simeq k^{-1}$. Similarly, each logarithmic interval contributes to the mean square gravitational potential the amount $\Phi^2=(k^3|\phi_k|^2/2\pi^2)$, where $\phi_k=4\pi G\Omega\rho_c(\delta_k/k^2)=(3H^2\Omega/2)(\delta_k/k^2)$. That is $\Phi^2=(3H^2\Omega/2)^2\,(P(k)/2\pi^2k)$.

The $\sigma^2(R)$ and Φ^2 also determine, in the linear regime, the probability distribution of density contrast and gravitational potential in a randomly chosen spherical region of radius R. For example, the probability that such a region has an average density contrast δ is given by

$$P[\delta]\,d\delta=[2\pi\sigma^2(R)]^{-1/2}\exp(-\delta^2/2\sigma^2(R))\,d\delta. \quad (2)$$

Similarly, the probability distribution for the gravitational potential ϕ is a gaussian with width $\Phi^2(R)$. These distributions, of course, will be modified in the nonlinear regime or in all regimes when the perturbations are nongaussian.

The models for the generation of density perturbations will provide us with the form of the function $P(k)$. A large class of models—including the inflationary models—lead to an initial spectrum of the form $P(k)=Ak$. For such a spectrum[7], (called 'Harrison–Zeldovich spectrum' or 'scale-invariant spectrum') the mean-square fluctuation in the gravitational potential $\Phi^2=(3H^2\Omega/2)^2\,(A/2\pi^2)$ is independent of k. This 'scale invariance' arises from the fact that the models which generate these perturbations do not possess any intrinsic length scale.

2.3 *The amplification of perturbations*

The small perturbations, once generated, will have a tendency to grow. Regions which are overdense will accrete more matter (or, equivalently, will expand more slowly compared to the background universe) and the density contrast will increase. In the initial stages of growth, when $\delta \ll 1$, the dynamics can be analysed using linear perturbation theory.

The linear perturbation theory[1,2] allows one to compute the power spectrum $P(k,t_f)$ at some time t_f, given the initial spectrum $P(k,t_i)=Ak$ at some $t=t_i\ll t_f$. (We have taken the initial spectrum to be scale-invariant, though most of our results will have a wider applicability.) It is often convenient to use the epoch of decoupling as a final reference point and set $t_f=t_{\rm dec}$; it is also usual to work with the quantity $\Delta(k,t)=(k^3\,P(k,t)/2\pi^2)^{1/2}$ rather than with $P(k,t)$. The form of $\Delta(k,t_{\rm dec})$ is then completely determined by the nature of the dark matter present in the universe.

Cosmological considerations[8], coupled with some recent laboratory experiments[9] suggest that any stable, weakly interacting, fermion which constitutes the dark matter must have a mass m which is either in the range of (10–100) eV or greater than about 35 GeV. Models in which $10\,\text{eV} \lesssim m \lesssim 100\,\text{eV}$ are called 'hot dark matter' (HDM) models while models with $m \gtrsim 35\,\text{GeV}$ are called 'cold dark matter' (CDM) models. In the HDM models, we have $\Omega_{\text{DM}} h^2 = (m/90\ \text{eV})$ and $\Delta^2(k, t_{\text{dec}})$ is given by[10]

$$\Delta^2(k, t_{\text{dec}}) = A(t_{\text{dec}})\, k^4 \exp\left[-4.61\ (k/k_{\text{FS}})^{3/2}\right], \qquad (3)$$

where $k_{\text{FS}} = 0.16\,\text{Mpc}^{-1}\ (m/30\,\text{eV})$ and $A(t_{\text{dec}})$ is an amplitude which is independent of k. In other words, the *shape* of the spectrum is completely determined by m. (Theoretical models in which perturbations arise from quantum fluctuations are not successful in predicting an acceptable value for A; it needs to be fixed by comparison with observation. Seeded models give a somewhat better handle on the amplitude. But even in these models, there exists a reasonable amount of freedom to adjust the numerical value.) In the CDM models, the variance is given[11] by

$$\Delta^2(k, t_{\text{dec}}) = \frac{A(t_{\text{dec}})\, k^4}{(1 + Bk + Ck^{3/2} + Dk^2)^2} \qquad (4)$$

with $B = 1.7\,(\Omega h^2)^{-1}$ Mpc, $C = 9\,(\Omega h^2)^{-3/2}$ Mpc$^{3/2}$ and $D = 1\,(\Omega h^2)^{-2}$ Mpc^2. (To be precise, this fitting formula reproduces the CDM results at scales larger than about 1 Mpc. At smaller scales the actual spectrum increases logarithmically.) Most of the seeded models[12] will give a spectrum which has more small scale power than the HDM spectrum.

If we normalize the CDM spectrum by setting $\sigma_8 \equiv \sigma(8\,h^{-1}\ \text{Mpc})$ to unity at $t = t_0$, we find that $A_0 = 4.4 \times 10^6$ for a universe with $\Omega = 1$, $\Omega_{\text{vac}} = 0$ $h = 0.5$. The CDM spectrum 'shifts' to larger length scales as $\Omega_{\text{DM}} h^2$ is decreased. If we consider a class of spectra, all normalized to the same value at, say, $R_0 = 8\ h^{-1}$ Mpc, then decreasing $\Omega_{\text{DM}} h^2$ will increase the power at $R > R_0$. This fact can be used to increase the power at large scales by keeping $\Omega_{\text{vac}} \neq 0$ and $\Omega_{\text{DM}} + \Omega_{\text{vac}} = 1$. For example, if $\Omega_{\text{DM}} \simeq 0.2$, $\Omega_{\text{vac}} \simeq 0.8$, $h = 0.7$ we get $A_0 = 25 \times 10^6$ with the same normalization $\sigma_8 = 1$; this is an increase by a factor 5 in large scale power.

Note that both the expressions (3) and (4) reduce to the form $\Delta^2 \propto k^4$ for small k (i.e. for large $R \simeq k^{-1}$) which corresponds to the shape of the initial spectrum. (Changing k^4 to k^{3+n} we can incorporate any other initial spectrum which is a power law.) For large k, the power is reduced considerably compared to the primordial spectrum. In HDM models, this occurs due to a phenomenon called 'free-streaming' which reduces the power exponentially at large k. In the CDM models, $\Delta^2(k)$ does increase with k but not as fast as the initial spectrum. It flattens to a constant value for $R \lesssim L_f$, where $L_f \simeq 4(\Omega h^2)^{-1}$ Mpc. This change of shape in the spectrum (compared to the initial spectrum) occurs[13] due to a process called 'stagexpansion'.

The above expressions, strictly speaking, refer to the power spectrum of dark matter. At $t < t_{\text{dec}}$, perturbations in the baryons do not grow since baryons are strongly coupled to the radiation. At $t \gtrsim t_{\text{dec}}$, baryons decouple from radiation and are influenced by the gravitational field of the perturbed dark matter. This leads to a rapid growth of baryonic density contrast and the equality $\delta_{\text{B}} \simeq \delta_{\text{DM}}$ is achieved fairly quickly.

For $t > t_{\text{dec}}$, the density contrast grows in proportion with the expansion factor: $\Delta(k, t) \cong (a(t)/a_{\text{dec}})\, \Delta(k, t_{\text{dec}})$ if $\Omega = 1$. (This fact is often used to specify the amplitude of the power spectrum in terms of the 'present' value $A_0 \equiv A(t_{\text{dec}})\,(1 + z_{\text{dec}})$ We shall follow this convention of specifying A_0, rather than $A(t_{\text{dec}})$, when no confusion will arise). For models with $\Omega \neq 1$ the growth of perturbations is more complicated. A reasonable approximation[12] will be $\Delta(z) = \Delta(z; \Omega = 1)\ (\Omega(z)/\Omega)^{0.65}$, where $\Omega(z)$ corresponds to the value $[\rho(z)/\rho_c(z)]$ at a redshift z. In a universe with $\Omega < 1$ the growth effectively ceases at $(1 + z_c) \simeq \Omega^{-1}$. Thus, to obtain a given density contrast today, we need a larger $A(t_{\text{dec}})$ in a $\Omega < 1$ universe compared to that in a $\Omega = 1$ universe.

As soon as $\Delta \simeq 1$ at some scale k, the linear theory breaks down around that scale and we need to do a nonlinear analysis. We shall now consider several aspects of nonlinear density growth.

In the HDM models, it is the scale $k_c = 0.694\, k_{\text{FS}}$ (at which Δ is maximum) which will go nonlinear first. Since a region with a size R will contain a mass of $M(R) = 1.17 \times 10^{12}\ M_\odot\ (\Omega h^2)(R/1\ \text{Mpc})^3$ in the matter-dominated phase, the first nonlinear structures which form in HDM models will have characteristic masses of about $M_c \simeq 4 \times 10^{15}\ M_\odot\ (m/30\,\text{eV})^{-2}$. This mass corresponds to that of large clusters; smaller structures, like galaxies, have to form by fragmentation of these objects in the HDM models.

The evolution is very different in CDM models. Since $\Delta(k)$ is a (gently) increasing function of k, the small length scales (corresponding to large k) will go nonlinear first. The structures will form hierarchically with larger scales going nonlinear at later times. There will also be considerable amount of merging and 'cross-talk' between the various scales. It is possible to capture some features of the nonlinear stage of the hierarchical clustering by the following scaling relations. Suppose we approximate some region of the power spectrum as $P(k) \propto k^n$, where n is a 'local' index. (For the CDM spectrum, $n = 1$ at large scales and varies continuously to $n = -3$ at very small scales. For galactic scales $n \simeq -2$.) Then $\Delta^2(k, t) \propto a^2(t)\, k^{n+3} \propto t^{4/3}\, k^{n+3}$ for $t > t_{\text{dec}}$; thus we see that a scale k goes nonlinear at a time $t_{nl}(k) \propto k^{-3(n+3)/4}$. These structures will have a

size of $L \propto k^{-1} a(t_{nl}) \propto k^{-1} t_{nl}^{2/3} \propto k^{-(n+5)/2}$ and a density of $\rho \propto t_{nl}^{-2} \propto k^{+3(n+3)/2} \propto L^{-3(n+3)/(n+5)} \propto L^{-\gamma}$. The constant of proportionality in any of these relations can be fixed if we know the scale which is going nonlinear today; that is, the value of k for which $\Delta^2(k, t_0)$ is unity. Observations suggest that this occurs at around $k_c \simeq (8\,h^{-1}\,\mathrm{Mpc})^{-1}$. Also note that these relations imply the scaling $v \propto (GM/L)^{1/2} \propto L^{(1-n)/(n+5)} \propto M^{(1/12)(1-n)}$ between the velocity dispersion v and mass M of a system. For galactic scales with $n \simeq -2$, we get $v^4 \propto M$ which is borne out by observations to a certain extent.

Somewhat more detailed modelling of nonlinear dynamics is possible using the concept of correlation function $\xi(\mathbf{x}, t)$ which is the Fourier transform of the power spectrum:

$$\xi(x,t) = \int \frac{d^3\mathbf{k}}{(2\pi)^3} P(k,t)\, e^{i\mathbf{k}\cdot\mathbf{x}} = \int_0^\infty \frac{dk}{k} \Delta^2(k,t) \left(\frac{\sin kx}{kx}\right). \tag{5}$$

To an excellent approximation, $\xi(x,t)$ and $\sigma(x,t)$ are related to each other by

$$\sigma^2(x,t) \cong \frac{3}{x^3} \int_0^x \xi(y,t)\, y^2\, dy. \tag{6}$$

The behaviour of ξ and σ^2 in the extreme linear and nonlinear limits is easy to determine. In the extreme linear case, $\sigma^2(x,t) \propto \xi(x,t) \propto a^2(t)\, x^{-(n+3)} \propto t^{4/3} x^{-(n+3)}$. In the extreme nonlinear case, bound structures with fixed proper radius $l = a(t)\, x$ will not participate in cosmic expansion. At a fixed l, $\sigma^2 = \langle(\delta\rho/\rho_b)^2\rangle$ must now grow as $(a^6/a^3) = a^3$. The a^6 factor arises from the fact that the background density ρ_b decreases as a^{-3} and $\sigma^2 \propto \rho_b^{-2}$; the a^3 factor in the denominator arises from the fact that in all samples of proper radius l used in taking the average, only a fraction proportional to a^{-3} will contribute to ξ. Thus, in the nonlinear regime $\xi(t,x) \propto \sigma^2(t,x) \propto a^3(t)\, F(a(t)\, x)$. The form of F can be determined by matching the linear and nonlinear expressions at $\xi = 1$. This will lead to the result that $\xi_{nl} \propto a^3\,[ax]^{-\gamma}$ with $\gamma = 3(n+3)/(n+5)$. Thus,

$$\xi_{\mathrm{lin}}(t,x) \propto a^2(t)\, x^{-(n+3)};$$

$$\xi_{\mathrm{nl}}(t,x) \propto a^3\,[ax]^{-\gamma} \propto a^{6/(n+5)}\, x^{-3(n+3)/(n+5)}. \tag{7}$$

This relation connects the index of the nonlinear regime with that of the linear regime. Notice that, in the range $n > -2$, the nonlinear correlation function grows more *slowly* compared to the linear spectrum.

The transition between the linear and nonlinear regimes is more difficult to analyse and one has to usually resort to numerical simulations[14]. It is, however, possible to make some progress along the following lines[15]: Since the mean number of excess neighbours of any particle is given by

$$N(x\,t) = (n, a^3) \int_0^x 4\pi y^2\, dy\, [1 + \xi(y,t)], \tag{8}$$

where n is the proper number density, the conservation law for pairs implies

$$\frac{\partial \xi}{\partial t} + \frac{1}{ax^2} \frac{\partial}{\partial x} [x^2 (1 + \xi)\, v] = 0 \tag{9}$$

with v denoting the mean relative velocity of pairs. (For a derivation of equations (8) and (9) see Peebles[1].) Using equation (6), it is easy to obtain an equation for σ^2:

$$a \frac{\partial}{\partial a} [1 + \sigma^2(a,x)] = \left(\frac{v}{-\dot{a}x}\right) \frac{1}{x^2} \frac{\partial}{\partial x} [x^3 (1 + \sigma^2(a,x))]. \tag{10}$$

It is now clear that the behaviour of $\sigma^2(a,x)$ is essentially decided by the dimensionless ratio $h(a,x) \equiv [v(a,x)/(-\dot{a}x)]$ between the relative velocity v and the Hubble velocity $\dot{a}x = (\dot{a}/a)\, x_{\mathrm{prop}}$. In the linear limit, when $\sigma^2 \ll 1$, linear perturbation theory[1,2] can be used to show that $h(a,x) \cong (2/3)\sigma^2$; in the extreme nonlinear limit ($\sigma^2 \gg 1$) bound structures would have formed in which v will balance out Hubble expansion: that is $v = -\dot{a}x$ implying $h \cong 1$. Since there is no intrinsic length scale in the problem, it seems reasonable to assume that h depends on a and x only through some universal function $h = h(\sigma^2)$ which has the asymptotic behaviour derived above. Of course, this assumption has to be ultimately checked by comparing the results with the numerical simulations[15,16].

When $h(a,x) = h[\sigma^2(a,x)]$, it is possible to find a useful solution to equation (10). It is straightforward to verify that the solution $\sigma^2(a,x)$ is determined by the relation

$$\int \frac{d\sigma^2}{h(\sigma^2)(1+\sigma^2)} = \ln\left[\, a^3 \{x^3(1+\sigma^2)\}^m \,\right], \tag{11}$$

where m is a constant. When $h(\sigma^2) \simeq (2/3)\sigma^2$ and $\sigma^2 \ll 1$, we can ignore σ^2 compared to $\ln\sigma^2$ and this relation gives the linear theory result: $\sigma_L^2 \propto a^2 x^{2m}$. Clearly $m = -(n+3)/2$ if $P(k) \propto k^n$. On the other hand, when $h \simeq 1$, $\sigma^2 \gg 1$, we get

$$\sigma^2 \propto (a^3 x^{3m})^{1/(1-m)} \propto a^3 (ax)^{3m/(1-m)} \propto a^3 (ax)^{-\gamma}, \tag{12}$$

where $\gamma = 3m/(m-1) = 3(n+3)/(n+5)$. From equation (6) we find that the same scaling behaviour holds for ξ. Thus the limiting forms derived earlier arise from the behaviour of $h(\sigma^2)$. Also note that the right-hand side of equation (11) is a function of $\sigma_L^2(a, l = x(1+\sigma^2)^{1/3}) \propto$

$a^2x^{2m}(1+\sigma^2)^{2m/3}$, which is the density contrast $\sigma_L(a,l)$ in the linear theory *evaluated at* the scale $l=x(1+\sigma^2)^{1/3}$. Thus we can write

$$\sigma_L^2[a,l]=\exp\frac{2}{3}\int\frac{d\sigma^2}{h(\sigma^2)(1+\sigma^2)}. \tag{13}$$

Since the original power law index has disappeared, this relation suggests that $\sigma_L^2(a,l)$ is a universal function $\sigma^2(a,x)$. To determine the behaviour of this function we need to specify $h(\sigma^2)$. Numerical simulations[16] show that $h(\sigma^2)$ has a single maximum (and hence overshoots $|v|=\dot{a}x$ before falling back) at about $\sigma^2\simeq(8-15)$ with $h_{\max}\simeq(1.5\text{–}2)$. The simplest model[15] for such a function with correct asymptotic behaviour will be:

$$h(\sigma^2)=\frac{2}{3}\sigma^2\frac{(1+\lambda\sigma^2)}{(1+(2/3)\lambda\sigma^4)} \tag{14}$$

with one free parameter λ. Integrating equation (13), we find that

$$\sigma_L^2(a,l)=\sigma^2(1+\lambda\sigma^2)^{(3\lambda+2)/3(1-\lambda)}(1+\sigma^2)^{-(3+2\lambda)/3(1-\lambda)}, \tag{15}$$

where $\sigma^2=\sigma^2(a,x)$. Best agreement with the numerical results is achieved for $\lambda\simeq0.36$ for which

$$\sigma_L^2(a,l)=\sigma^2(1+0.36\sigma^2)^{1.604}(1+\sigma^2)^{-1.937}. \tag{16}$$

Figure 1 shows the function $\sigma^2(\sigma_L^2)$; also shown is a multiparameter fit[17] to the numerical data given by

$$\sigma_L^2=\sigma^2\left[\frac{1+0.0158\sigma^4+0.000115\sigma^2}{1+0.926\sigma^4-0.0743\sigma^6+0.0156\sigma^8}\right]^{1/3}. \tag{17}$$

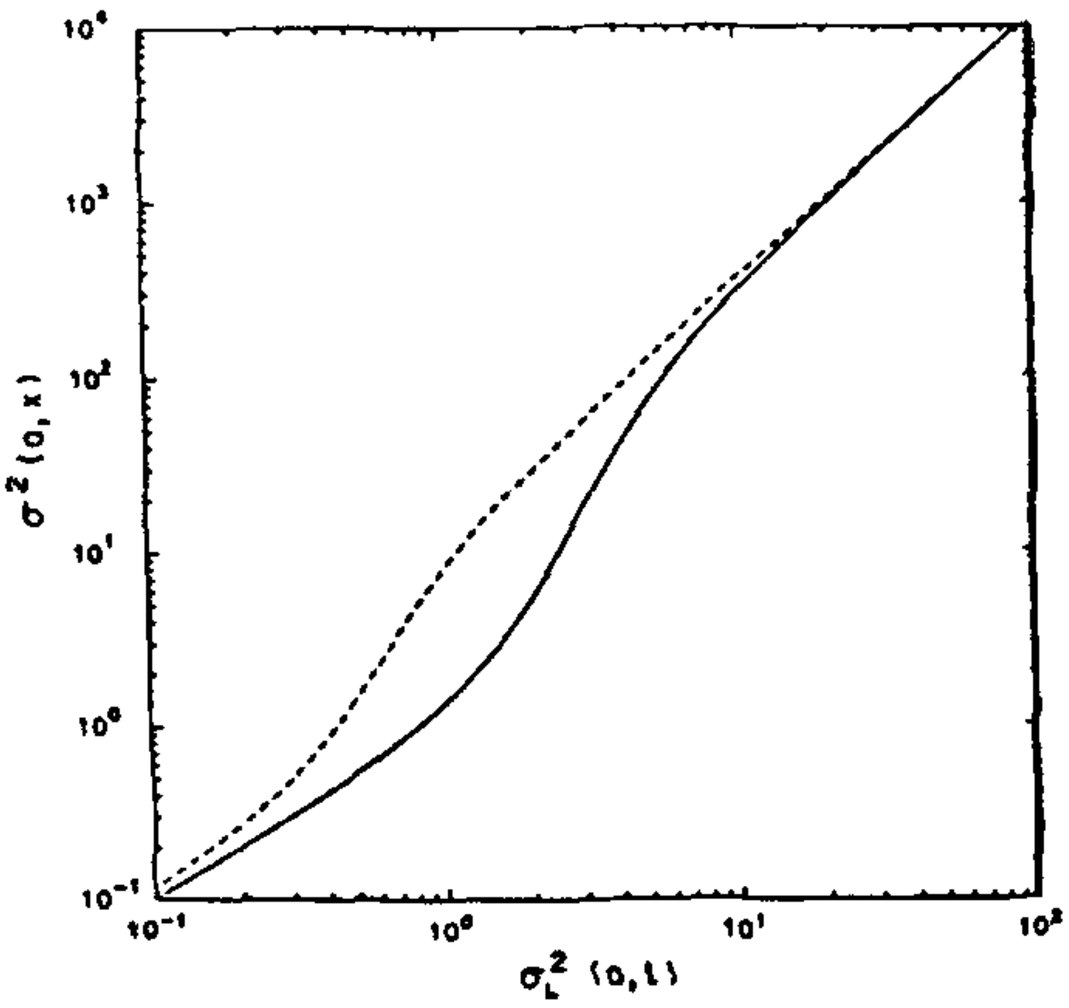

Figure 1. The nonlinear mass fluctuation $\sigma^2(a,x)$ is plotted against the linear mass fluctuation $\sigma_L^2(a,l)$ evaluated at $l=x(1+\sigma^2)^{1/3}$. The solid line shows the 'universal' best fit to numerical simulation given in ref. 17. The broken line is based on the theoretical model discussed *in the text.*

It is remarkable that the single parameter fit in equations (14), (16) is reasonable for all $\sigma^2\gtrsim6$ and for $\sigma^2\lesssim0.2$. The deviation in the intermediate range is due to the fact that equation (16) has the behaviour $(\sigma_L/\sigma)^2=1+\mathcal{O}(\sigma^2)$ while the actual data suggest $(\sigma_L/\sigma)^2=1+\mathcal{O}(\sigma^4)$ for $\sigma_L^2\gtrsim10$.

It should be stressed that σ_L^2 and σ^2 in the above formulas are evaluated at different length scales. The relation of σ^2 to σ_L^2 at the *same* length scale is quite complicated and depends on the shape of the spectrum. For example, in the extreme nonlinear limit,

$$\sigma^2(x,a)\simeq11.4^{2/(n+5)}a^{6/(n+5)}(x/x_0)^{-\gamma}$$

$$\simeq11.4^{2/(n+5)}\ a^{-2(n+2)/(n+5)}\sigma_L^2(x,a)(x/x_0)^{\beta} \tag{18}$$

with $\beta=[(n+3)(n+2)]/(n+5)$, $\gamma=3(n+3)/(n+5)$ and $x_0\simeq8\,h^{-1}$ Mpc. For a CDM spectrum, galactic scales have $n\simeq-2$ and smaller scales have $n\simeq-3$. So the nonlinear density contrast is a factor of about 11 larger at subgalactic scales and a factor of $11^{2/3}$ higher at galactic scales. This has the effect of steepening the correlation function at the nonlinear end.

The statistics of the density contrast, described by the probability distribution $\mathscr{P}[\delta]$, will also change in the nonlinear regime. Since the density has to be positive definite, we must have $\mathscr{P}[\delta]=0$ for $\delta<-1$. (This restriction, of course, exists in the linear regime as well but since $\mathscr{P}[|\delta|=1]\ll1$ in the linear regime it makes no practical difference.) Further, once nonlinear clumps have formed, most of the region in the universe will be underdense; thus $\mathscr{P}[\delta]$ will be peaked around $\delta\gtrsim-1$ with a long tail for positive δ. The probability distribution will go over to the gaussian form of the linear theory if a large filtering scale is used.

It is possible to evaluate the nonlinear probability distribution in an approximate manner and verify the above conclusions. One such study[18] shows that the probability $\mathscr{P}[\delta;L]$ at the filtering scale L is

$$\mathscr{P}[\delta;L]=\frac{N}{\sqrt{2\pi}\,\sigma_0(\delta)}\frac{1}{(1+\delta)^{7/3}}$$

$$\exp\left[-\frac{9}{2\sigma_0^2(\delta)}\left(1-\frac{1}{(1+\delta)^{1/3}}\right)^2\right], \tag{19}$$

where N is a normalization constant and $\sigma_0(\delta)$ stands for the variance calculated from the linear theory evaluated at $R=L(1+\delta)^{1/3}$. It is easy to verify from

equation (19) the following facts: (i) When the filtering scale L is large, $\sigma \propto L^{-2}$, and $\mathscr{P}$ reduces to the linear theory result. (ii) In general $\mathscr{P}$ is much more sharply peaked and has a mean value shifted towards $\delta < 0$. (iii) For small filtering scales (i.e. when $L \to 0$), the variance σ_0^2 effectively becomes a constant (in non-HDM models) and $\mathscr{P}[\delta; L]$ becomes sharply peaked at $\delta \simeq -1$. These results agree with the expectations mentioned in the last paragraph.

The discussion above concentrated on the dynamical effects due to gravity alone. The evolution of baryons in the nonlinear stage is much more complicated because they can cool by radiating energy. The effect of such processes will be to make baryons sink to the bottom of the dark matter potential wells, thereby segregating dark matter and baryons. Several complicated hydrodynamical effects can arise during this stage and we do not have today a systematic understanding of such an evolution[2,12]. These processes, in particular, can make the statistical behaviour of luminous matter very different from that of underlying dark matter distribution. Since the study of density distribution at small scales is invariably based on luminous galaxies, this fact creates considerable difficulties in interpreting the observational data.

3. Observational background

We shall now review a series of observational results which any model for structure formation must explain. In each case, we shall briefly indicate the status of theoretical models in explaining the observations. A more global comparison will be attempted in section 4.

3.1 *Distribution of galaxies*

The most direct measure of inhomogeneities in the universe is provided by galaxy surveys[19]. These surveys can be broadly classified as follows: (i) Fairly complete, all-sky, three dimensional surveys like the CfA, IRAS and QDOT surveys. (ii) Two-dimensional surveys (like APM survey) which contain information about the angular distribution of galaxies in the sky but lack actual redshift information. (iii) Pencil-beam surveys which could provide information along particular directions in the sky. The depth of such pencil beam surveys can be fairly high, though the sky coverage is somewhat limited.

One useful statistic that can be extracted out of such surveys is the correlation function $\xi(r)$ or equivalently, the density contrast $\sigma(r)$. This information is directly available in three-dimensional surveys; in two-dimensional surveys it is possible to extract this information from the angular correlation function $W(\theta)$. Pencil beam surveys usually do not possess sufficient spread to allow reliable computation of $\xi(r)$. Hence these surveys often rely on purely visual impressions in the interpretation of data.

The $\sigma(r)$ obtained[20] from some of the galaxy surveys is shown in Figure 2. It is clear that $\sigma(r) \simeq 1$ at $r = r_c \simeq 8\,h^{-1}$ Mpc, suggesting that linear theory is applicable for $r \gg r_c$. The correlation function $\xi_{gg}(r)$ corresponding to this data is well approximated by $\xi_{gg}(r) = (r/5\,h^{-1}\,\text{Mpc})^{-1.8}$ for $0.1\,h^{-1}$ Mpc $< r < 20\,h^{-1}$ Mpc. (Note that the QDOT results (filled triangles) use *cubical* cells of side R in computing $\sigma(R)$, while the others are based on spheres of radius R. This leads to a systematic shift. A more detailed comparison of QDOT with other data is in progress.) Since galaxy surveys contain information up to $60\,h^{-1}$ Mpc or so it may seem that we can, in principle, compare the linear theory with the observation over a reasonable range. There is however, one major difficulty: The information in galaxy surveys comes from the luminous, baryonic part of the galaxies. It is not obvious that the statistical properties of the luminous part will be the same as that of the underlying mass distribution. For example, it could happen[21] that galaxies form at those regions of space where the density contrast is much higher than the average; in that case, the galaxy–galaxy correlation function $\xi_{gg}(r)$ will be larger than the underlying mass correlation function $\xi(r)$. It is usual to write $\xi_{gg}(r) = b^2 \xi(r)$ (with $b > 1$), where b is called the biasing factor. There

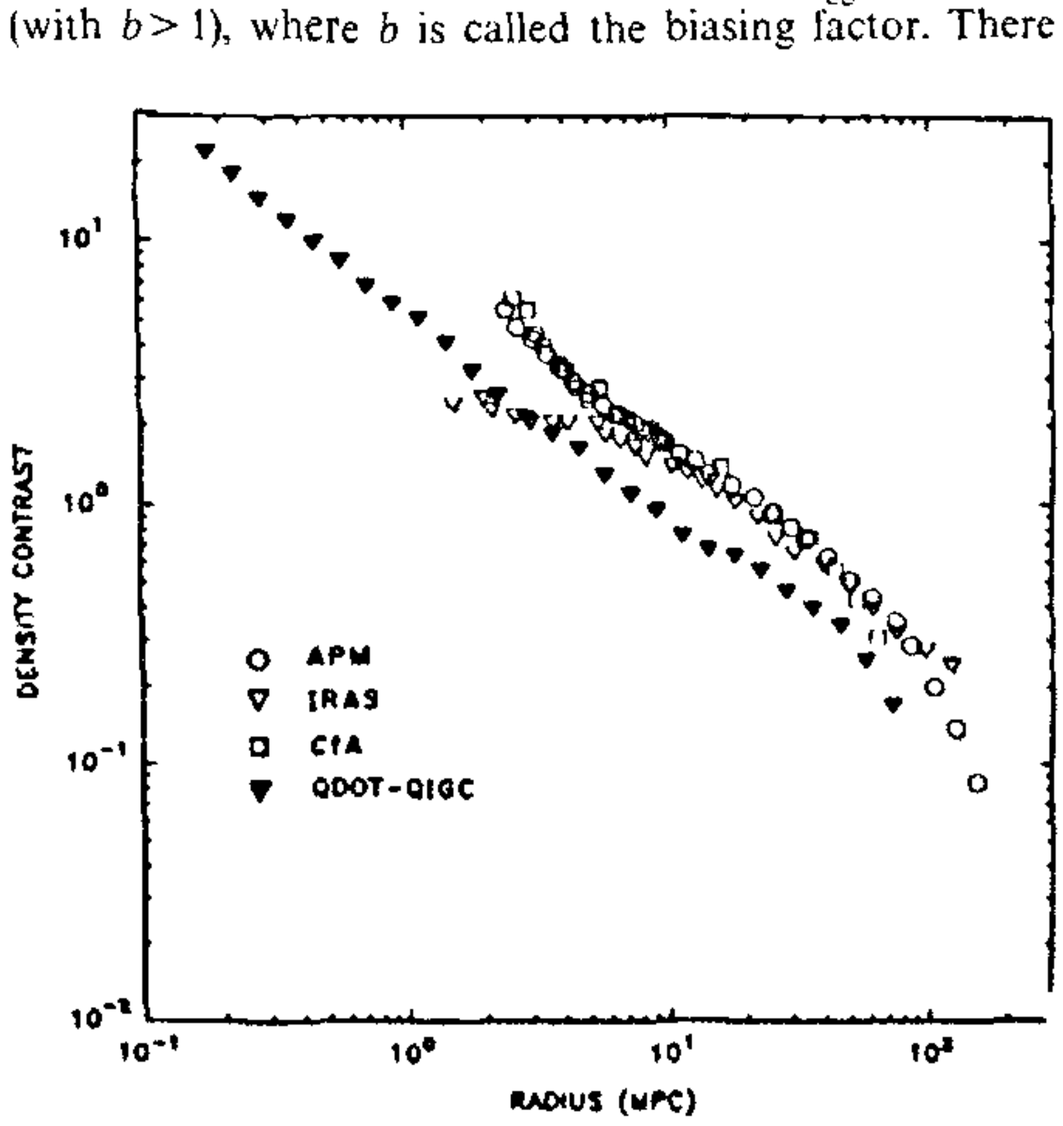

Figure 2. The density contrast $\sigma(R) = \langle (\delta M/M)_R^2 \rangle^{1/2}$ determined from various galaxy surveys (see ref. 20). APM (circles), IRAS (open triangles), CfA (squares) and QDOT (filled triangles). The QDOT results are based on counts in *cubical* cells of size R while the other three results are based on spheres of radius R, which could partly account for the systematic shift. The QDOT data were kindly provided by Rowan Robinson and is based on Saunders, W. *et al.*, 1992 (Oxford preprint OUTAS 92/4, to be published). We have set $h = 0.5$.

could[22] also be other effects—like the dynamical friction—which could make b less than unity. What is more, since the astrophysical processes which operate at different scales are different, the factor b could even be function of r. This possibility could seriously reduce the predictive power of the theory unless we understand clearly the processes which could segregate luminous matter from dark matter. Usually, one *assumes* that b is a constant and tries to determine it by comparing the theory with observations.

These attempts have led to somewhat divergent results. To begin with, numerical simulations[23] of nonlinear growth show that it is extremely difficult to make the correlation functions in HDM models to agree with ξ_{gg}. The difficulty arises mainly because of the following fact: HDM models have a characteristic scale of about $25\,h^{-1}$ Mpc. When galaxies form due to fragmentation of larger structures, this scale is imprinted on the galaxy distribution. The observed scale in ξ_{gg} is about $5\,h^{-1}$ Mpc. It follows that HDM will lead to a galaxy distribution which is much more clustered than is observed.

In CDM models it is possible to obtain an agreement[24] between observation and theory provided $b \simeq (2\text{–}2.5)$ and $h \simeq 0.5$. The steepening of the correlation function in the nonlinear scales, discussed earlier, plays a crucial part in obtaining this result. The CDM models, however, run into trouble[25] at larger scales (around $r \gtrsim 40$ Mpc). Since the biasing was chosen to match the distribution at small scales, the $\sigma(r)$ at large scales falls considerably short of the observed results. For example, if we set $\sigma(8\,h^{-1}\,\text{Mpc}) = (1/b)$, then we find that $\sigma(50\,h^{-1}\,\text{Mpc}) \simeq (0.1/b)$. This is a factor 2 below the observation even if we take $b=1$. Note that we are actually concerned here with the *shape* of the CDM spectrum in these observations; the discrepancy shows that the shape is wrong. One obvious way out of this dilemma will be to make b scale-dependent, thereby allowing σ_{gal} to have a shape different from σ_{CDM}; i.e. $\sigma_{gal}(R) = \sigma_{CDM}(R)/b\ (R)$. Unfortunately, this will take away the predictive power of the theory. Alternatively, one can try to normalize the spectrum at large scales, say at $50\,h^{-1}$ Mpc. We have to then invoke some (unknown) nonlinear effect to *reduce* the σ at small scales. This difficulty is probably the most difficult challenge faced by all the galaxy formation models. We shall discuss several related aspects of this problem in what follows.

Incidentally, all the surveys show that $\langle (\delta M/M)_R^2 \rangle$ is a decreasing function of R thereby confirming our basic assumption that the universe can be described—at sufficiently large scales—by a Friedmann model.

3.2 *Galaxy counts*

Observations of low redshift samples of the galaxies suggest that the galaxy luminosity function has the form

$$\Phi(L)\,dL\,dV = \Phi_0 (L/L_0)^{-\alpha} \exp(-L/L_0)(dL/L_0)\,dV \tag{20}$$

with $\Phi_0 \simeq 0.012\,h^3\,\text{Mpc}^{-3}$, $L_0 \simeq 10^{10}\,h^{-2}\,L_\odot$ and $\alpha \simeq (1.1\text{–}1.2)$. Recently, there has been significant progress in the counts of very faint galaxies[26]. These observations are now available up to $B=27$ magnitude in blue (corresponding to 7×10^{-31} erg cm^{-2} Hz^{-1} at 4500 Å) and up to $K=23$ magnitude in infrared (corresponding to 4×10^{-30} erg cm^{-2} Hz^{-1} at 22000 Å). For galaxies with magnitude up to $B=24$ or so, the median redshift appears to be around 0.4. In general, these counts lead to far more faint galaxies than can be accounted for in simple models, especially beyond a magnitude of about $B=21$. For example, there are about 4.5×10^5 galaxies per square degree which are brighter than the 27th magnitude; this is a factor 5 to 10 higher than what is expected from the luminosity function for most cosmological models. The counts also show that the disparity is different in different wavebands. The latter fact suggests that one cannot account for higher counts by setting $\Omega_{vac} \neq 0$ so that more cosmological volume is available at the redshifts of $z \simeq (0.3\text{–}0.6)$.

At present two different explanations have been suggested for the observed abundance of faint galaxies: (i) One may assume that there has been significant amount of galactic mergers in the low redshift universe. This would naturally lead to more galaxies at higher redshifts than expected from a low-z luminosity function. (ii) More generally, one may assume that there was significant amount of evolution in the galaxy luminosity function at low redshifts. Observations seem to suggest that such an evolution should depend not only on the luminosity of the galaxy but also should differ from band to band. Both these models face difficulties and at present it is not clear whether we can explain all the faint galaxy counts by a realistic model[27].

3.3 *High redshift objects*

There is mounting evidence to suggest that significant amount of structure formation must have taken place at redshifts even as high as $z \simeq 4.5$. This evidence comes from essentially five different kinds of observations.

(i) Quasars have been seen[28] up to a redshift of about $z \simeq 4.9$ and there are more than thirty quasars with a redshift larger than 4. If the conventional models for the quasar luminosity are correct, then the galactic cores containing these quasars must[29] have a mass of $M_Q \gtrsim 10^{10}\,M_\odot$. Thus the mass scales of $M \simeq (10^{10}$–

$10^{11}) M_\odot$ should have gone nonlinear at a redshift of $z \gtrsim 4$. From theoretical models, one can relate the collapse redshift $z_c(M)$ for a mass M, to the density contrast $\delta_L(M)$ computed using linear theory. Most models suggest $(1+z_c)=(\delta_L/\delta_{cri})$ where $\delta_{cri} \simeq (1.5\text{–}2)$. Figure 3 shows the mass which will collapse at various redshifts in the standard CDM model with $b=2$. It is clear that the model has some difficulty in accounting for the data.

(ii) The study of absorption lines of quasars shows that there exist[30] bound clouds of neutral hydrogen (with masses of about $(10^8\text{–}10^{11}) M_\odot$) at redshifts $z \simeq 2.5\text{–}3.5$. Several of these absorption line systems indicate the presence of heavy elements, suggesting that the universe at high redshifts should possess fairly evolved structures in reasonable quantities. At present, we have absorption data on Mg II at $z=(0.3\text{–}1.5)$, on C IV at $z=(1\text{–}3)$, on Lyman limit systems at $z=(0.6\text{–}3.5)$, on narrow, sharp, Lyman -α lines at $z=(1.7\text{–}4)$ and on damped Lyman -α lines at $z=(1.7\text{–}3.5)$. For each of these absorption systems, one knows the number density per unit redshift range as well as the distribution of hydrogen column density. By and large, these number densities are significantly higher (by factors of 10 to 100) than what would be expected in a model with $\Omega=1$, $h=0.5$ and $\Omega_{vac}=0$, if we assume that the comoving density of absorbers is conserved. These observations have to be accounted for in any scenario for structure formation.

(iii) Quasars can be used to probe the existence (or otherwise) of smooth distribution of neutral hydrogen in the universe. Any such distribution will lead to a dip in the spectrum on the blue side of the Lyman alpha emission line. No such dip is seen, allowing[31] us to conclude that the density of neutral hydrogen—distributed smoothly in the universe—must be less than about $n_H \cong 8.4 \times 10^{-12} h \text{ cm}^{-3}$ at a redshift of $z \simeq 2.64$. This is to be compared with the baryon density at this redshift, which is about $n_B \simeq 2 \times 10^{-4} (\Omega_B h^2)$ cm^{-3}. Similar results hold for quasars with higher redshifts. Since the standard Friedmann model predicts that neutral atoms were formed at about $z_{dec} \simeq 1100$, it follows that the smooth component of hydrogen must have been reionised sometime in the redshift interval $z_{dec} > z > 4$. (An alternative hypothesis would be that galaxy formation was extremely efficient and formed lumps out of *all* hydrogen; this is virtually impossible to achieve in any sensible theoretical model.) Consequently, at least some structures must have formed at $z \gtrsim 5$, evolved by a reasonable amount and emitted sufficient quantity of UV photons to reionise the hydrogen. This provides another, indirect, evidence for early structure formation. At present, however, there is no satisfactory theoretical model for the source of ionising flux[32].

(iv) Several radio galaxies have been detected[33] with a redshift of $z \gtrsim 2$. Though the mass estimate of these galaxies is somewhat model-dependent, most reasonable models give $M \gtrsim 10^{11} M_\odot$. This could probably be the most direct evidence we have for star-forming galaxies at $z \gtrsim 2$.

(v) There exists[34] a single observation of redshifted 21 cm line emission from a cloud of neutral hydrogen at a redshift of $z=3.397$. The width of the line suggests that the velocity dispersion in the cloud is about $v \simeq 180 \text{ km s}^{-1}$. From the observed flux of $S=11.4$ mJy, one can estimate the mass of this cloud to be $M_H = 2.2 \times 10^{13} h^{-2} M_\odot$, if $\Omega=1$ and $M_H = 6.9 \times 10^{13} h^{-2} M_\odot$ if $\Omega=0.1$. (The *total* mass can be a factor ten higher.) Theoretical models predict that the characteristic velocity σ for such an object will be about $\sigma \simeq 1400 \ (M/10^{15} M_\odot h^{-1})^{1/3} \text{ km s}^{-1}$ if it is spherically symmetric. The fact that $v \ll \sigma$ suggests that either the object is far from spherically symmetric or it is seen during a special epoch in its evolution[35].

The first possibility will arise naturally in the HDM models in which masses of about $10^{14} M_\odot$ will go nonlinear first. Further evolution can produce pancake-like structures with highly anisotropic velocity dispersion. Unfortunately, the MBR anisotropy detected by COBE restricts the power spectrum of pure HDM models, making it highly improbable that these objects could have formed at $z \gtrsim 2$. (We will discuss the COBE bounds in section 3.5). The second possibility can be realized if we interpret this object as a part of the protocluster of galaxies and assume that it is seen just after it has turned around, when its velocity will be much lower than the virial velocity σ. However, the

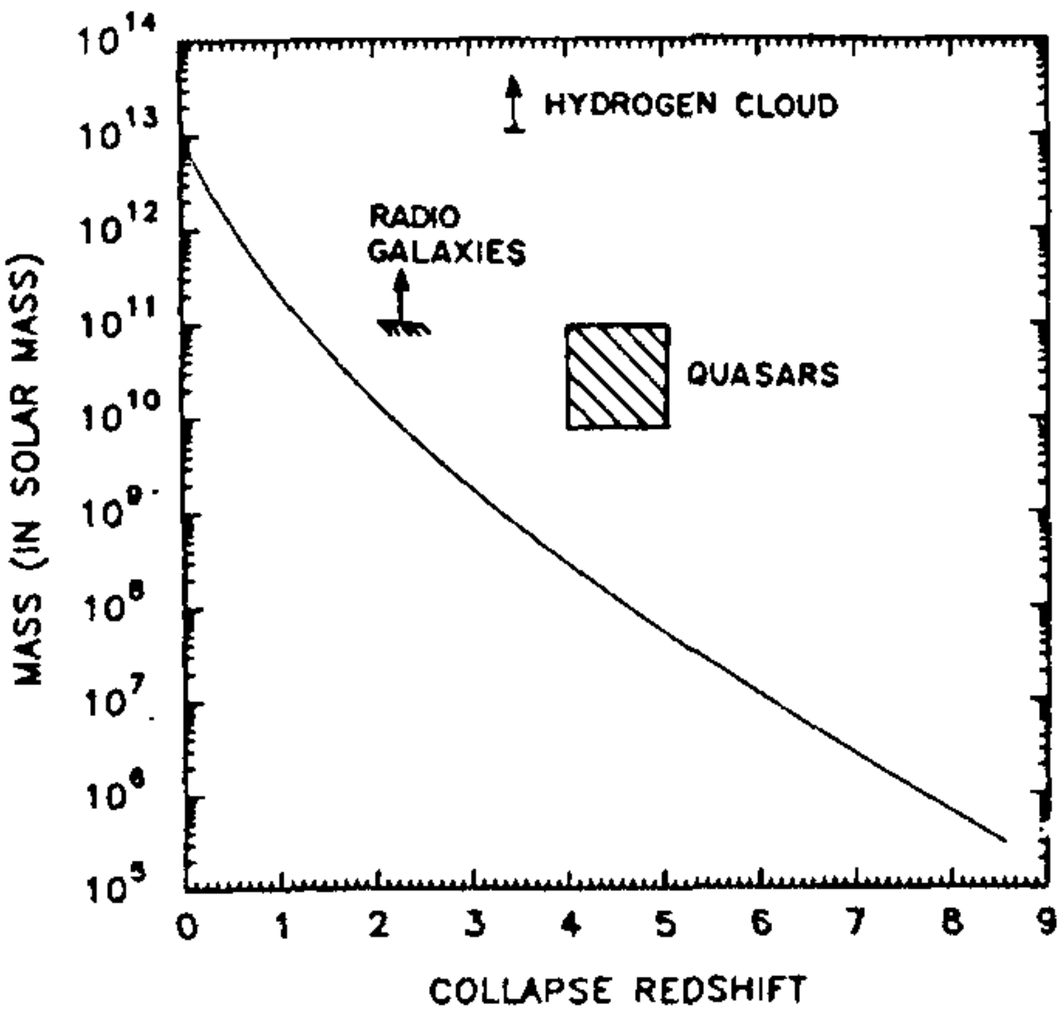

Figure 3. The mass scale which goes nonlinear at various redshifts is shown for a CDM model with $\sigma_8 \simeq 0.5$, $h=0.5$. Also shown are the masses of several high redshift objects.

probability for the occurrence of such a fortuitous circumstance is also very low. The detection of larger number of such objects could pose serious problems for many scenarios of structure formation.

3.4 *Large scale streaming*

In a strictly homogeneous universe, galaxies will only have Hubble velocities. The deviation $\delta\rho(\mathbf{x},t)$ of the density from the uniform value will induce velocities to observed structures over and above the Hubble velocity. The magnitude of this velocity (called 'peculiar velocity' or 'streaming velocity') is easy to estimate in the linear theory. If the excess mass in a region of size R is $\delta M(R)$ then the average peculiar velocity $v(R)$ in this region will be $v(R) \cong gt \cong t(G\delta M(R)/R^2) \cong (4\pi G/3)\, tR\,(\delta\rho) = (\Omega H_0 t/2)\, v_H(R)\, \delta(R)$, where $v_H(R) = H_0 R$ is the Hubble velocity and $\delta(R)$ is the density contrast at this scale. The quantity $f(\Omega) = (3H_0 t/2)\Omega$ is purely a function of Ω and is well approximated by $f(\Omega) \cong \Omega^{0.6}$. *Thus we get* $[v(R)/v_H(R)] \cong (1/3)\,\Omega^{0.6}\,\delta(R)$. Since $\delta \propto R^{-2}$ at large scales $v \propto R^{-1}$ for large R.

The peculiar velocity of our Local Group can be estimated reasonably accurately from the dipole anisotropy of the MBR (see next section) and is found[36] to be $v_{LG} \cong (622 \pm 20)$ km s^{-1} in the direction of $l = 277° \pm 2°$ and $b = 30° \pm 2°$. To measure the peculiar velocities of other, distant, galaxies one requires a distance indicator which is *not* based on Hubble's law. Most measurements in recent years use either the Tully-Fisher relation ($L \propto v^4$ where L is the absolute luminosity of a spiral and v is the rotational velocity) or the $D_n - \sigma$ relation ($D_n \propto \sigma^{4/3}$ where D_n is a suitably defined angular diameter of a spiral and σ is the central velocity dispersion). *Such measurements*[37] *of peculiar* velocities have led to the following conclusions: (i) There exists a large, bulk velocity of about 600 km s^{-1} within a region of 60 h^{-1} Mpc. A study[38] of the velocity field shows that v_{rms} (40 h^{-1} Mpc) = (388 ± 67) km s^{-1} and v_{rms} (60 h^{-1} Mpc) = (327 ± 82) km s^{-1}. (ii) The galaxies within a region of about 5 h^{-1} Mpc or so share the motion of the Local Group.

We see from Figure 2 that $\delta(50\, h^{-1}\ \text{Mpc}) \simeq 0.2$; this would imply that $(v/v_H) \simeq (1/3)\,\delta \simeq 0.067$ or $v(50\, h^{-1}$ Mpc$) \simeq 335$ km s^{-1}, which is in rough agreement with the v_{rms} quoted above. The detailed maps of density distribution obtained from velocity field, however, do not match with the one based on IRAS and QDOT surveys[39]. The cause for this discrepancy is not clear. *The fact that ellipticals make significant contribution to* velocity determinations but appear only marginally in the infrared selected samples could be one possible source of disparity.

While the galaxy surveys are in broad agreement with peculiar velocities, theoretical models have difficulty in accounting for v_{rms}. If we set $\sigma \simeq 1$ at $r_0 \simeq 10\, h^{-1}$ Mpc then $v \simeq v_H$ at $r = r_0$; so $v(r) \simeq 10^3$ km s^{-1} $(r/10\, h^{-1}\ \text{Mpc})^{-1}$ for large r, giving $v(60\, h^{-1}$ Mpc$) \simeq 166$ km s^{-1}. This is far short of the observed velocities. This discrepancy, of course, is to be expected because theoretical models have far less power at large scales compared to what is seen in galaxy surveys.

3.5 *Distortions in the microwave radiation*

The MBR photons reaching us today could contain information about the universe at $z = z_{dec} \simeq 10^3$ if they did not interact significantly with matter at $z < z_{dec}$. (The latter possibility can occur in models in which matter was reionised; we will discuss this case separately.) Physical processes which have a characteristic length scale L will distort the temperature distribution of radiation in the 'last-scattering-surface' (LSS) at the corresponding scale. This will, in turn, appear today as temperature anisotropy $S(\theta) \equiv (\Delta T/T)$ *in the sky at a characteristic angular scale* $\theta(L) \cong (\Omega/2)\ H_0(Lz) \simeq 34.4''\ (\Omega h)\ (L_0/1\ \text{Mpc})$, where $L_0 = L(1+z) \cong L_z$ is the corresponding scale today (we have assumed that $z \gg 1$). In particular, the Hubble radius at $t = t_{dec}$, $H_{dec}^{-1} \simeq ct_{dec}$, will subtend in the sky an angle of $\theta_H = \theta\ (H_{dec}^{-1}) \cong 0.87°\, \Omega^{1/2}\ (z_{dec}/1100)^{-1/2} \simeq 1°$. This shows that most microphysical processes (which operate at scales $L \ll H^{-1}$) can only affect $S(\theta)$ at $\theta \lesssim 1°$. Anisotropies at larger scales probe the primordial, gravitational distortions[40].

The MBR anisotropies at $\theta \lesssim 1°$ are of less importance compared to large angle anisotropies for two other reasons as well. We saw in section 3.3 (iii) that the matter in the universe was ionized sometime before the redshift of $z \simeq 5$. Since MBR photons could be scattered by ionized matter the ionization history of the universe could affect the predictions for the temperature anisotropies of the MBR. It turns out, however, that even in the worst possible case, of reionization of the universe can only affect anisotropies at angular scales less than $\theta_{ion} \simeq 7.4°$ $(\Omega_B \Omega_n)^{1/3}$. Thus the anisotropy at angular scales larger *than about 10° is safe from such distortion. Secondly, it* must be noted that the decoupling at $z \simeq 1100$ is not[41] an instantaneous event but takes place over a redshift interval of about $\Delta z \simeq 80$. This Δz corresponds to a length scale of about $\Delta l \simeq 15\Omega^{-1/2}$ Mpc and an angular scale of $\theta_{min} \simeq 8'\, \Omega^{1/2}\, h$. Thus it is anyway impossible to observe temperature anisotropies below, say, 5′.

The temperature anisotropies of MBR arise from essentially four different sources, which we shall discuss one by one. When the individual distortions are small, they can be added together to obtain the total anisotropy.

(i) The motion of the detecting apparatus with

respect to comoving frame (in which the MBR is, say, isotropic) will produce a 'dipole' anisotropy in the radiation. If the fractional deviation in sky temperature is expanded in spherical harmonics as, $(\delta T/T) \equiv S(\theta, \phi) = \Sigma_{l,m} a_{lm} Y_{lm}(\theta, \phi)$, then the motion of the detector contributes significantly to the $l=1$ term. Observations show that the dipole anisotropy is nearly hundred times higher than the anisotropy due to quadrupole and higher modes. For this reason, it is usual to subtract out the dipole term and consider only the rest of the contribution as intrinsic. Note, however, that the dipole anisotropy allows us to determine our motion with respect to the comoving frame; this was discussed in the last section.

(ii) If the energy density of radiation in the LSS has intrinsic spatial variation, then it will appear today in the sky as a temperature anisotropy. In most models of structure formation $(\delta\rho/\rho)_R \simeq (\delta\rho/\rho)_B$ at the LSS; in the inflationary models, for example, $(\delta\rho/\rho)_R \simeq (1/3)\,(\delta\rho/\rho)_B$. This will lead to a temperature distortion of $(\delta T/T)_I \simeq (1/3)(\delta\rho/\rho)_B = (1/3)\,\sigma_{DM}(L) f_1 (1+z_{dec})^{-1}$, where $\sigma_{DM}(L)$ is the linear density contrast of dark matter today and the factor $f_1 = (a_{eq}/a_{dec}) \simeq (1/20\,\Omega\,h^2)$ arises because dark matter perturbations can grow from $t = t_{eq}$ onwards. This formula, however, does not take into account the fact that the decoupling is not an instantaneous process but takes a redshift interval of about $\Delta z \simeq 80$ for its completion. This smearing reduces[40] the distortion by a further factor of about $f_2 \simeq 0.1$ in most models. Since $\sigma(50\,h^{-1}\ \mathrm{Mpc}) \simeq 0.2$, we get $(\delta T/T) \simeq 0.3\,h^{-2} \times 10^{-6}$ at the angular scale $\theta(50\,h^{-1}\ \mathrm{Mpc}) \simeq 0.5°$. Notice that the angular dependence of $(\delta T/T)$ is decided entirely by the shape of $\sigma(L)$; since $\sigma(L) \propto L^{-2}$ for large L, $(\delta T/T)_I \propto \theta^{-2} \simeq 0.3\,h^{-2} \times 10^{-6}\,(\theta/0.5°)^{-2}$.

(iii) The random velocities in the matter distribution at the LSS can induce Doppler shifts in the scattered photons, producing a velocity-induced anisotropy. This will give $(\delta T/T)_v \simeq (v/c)_{LSS}$. Since $v \simeq H^{-1}\,(\delta\phi/L)$, where $\delta\phi \simeq (2G\delta M/L) \simeq (\delta\rho/\rho_b)\,(HL)^2$, it follows that $(\delta T/T)_v \simeq (\delta\rho/\rho)(LH)$ evaluated at the LSS. Clearly $(\delta T/T)_v$ falls as θ^{-1} at large angles. A simple estimate gives $(\delta T/T)_v \simeq 10^{-5}\,(\theta/2°)^{-1}$.

(iv) The most dominant—and important—contribution to the anisotropy comes from the variation of the gravitational potential on the LSS (this is called 'Sachs–Wolfe effect')[42]. Since the photons climbing out of different potential wells undergo different amounts of redshift, we obtain a $(\delta T/T) \simeq (1/3)\,(\delta\phi/c^2)$. [The (1/3) factor may be interpreted as follows: The gravitational redshift produces $(\delta T/T) = (\delta\phi/c^2)$; time dilation gives $(\delta T/T) = -\delta a/a = -(2/3)(\delta t/t) = -(2/3)\,(\delta\phi/c^2)$. This interpretation, however, is highly gauge dependent.] Since $\delta\phi \simeq (\delta\rho/\rho)\,H^2 L^2$, we find that $(\delta T/T) \simeq (H^2/3)\,L^2\,\sigma(L)$. But since $\sigma \propto L^{-2}$ at large L, this leads to a $(\delta T/T)$ which is independent of 0. To estimate the magnitude of this effect, note that $\sigma \propto a(t)$, $L^2 \propto a^2(t)$ and $H^2 \propto \rho_b \propto a^{-3}(t)$ implying $\delta\phi(t_{dec}) = \delta\phi(t_0)$. The gravitational potential of largest bound structures today is $\delta\phi(t_0) \simeq 10^{-5}\,c^2$ giving $(\delta T/T) \simeq 3 \times 10^{-6}$. At $\theta \gtrsim 1°$, this is the most dominant effect, since the other two contributions fall with increasing θ.

The search for anisotropy in MBR has recently led to a positive result[43]. The analysis of data from the satellite COBE has now given the following numbers: (i) The dominant term is a dipole anisotropy of magnitude $(\Delta T/T)_{dipole} \cong 1.23 \times 10^{-3}$, towards the direction $l = 284.7° \pm 0.8°$, $b = 48.2° \pm 0.5°$. We saw earlier that such an effect arises due to purely kinematic reasons. (ii) The root-mean-square fluctuation in temperature, in the angular range of 15°–165°, is found to be $(\Delta T/T)_{rms} = (1.1 \pm 0.2) \times 10^{-5}$. (iii) The quadrupole contribution to the anisotroy is $(\Delta T/T)_Q = (0.48 \pm 0.15) \times 10^{-5}$. These results have important implications for the models of structure formation which we shall now discuss[44].

It can be shown that[45] the mean square anisotropy, $(\Delta T/T)^2_{rms}$, and the quadrupole contribution, $(\Delta T/T)^2_Q$, from Sachs–Wolfe effect are given by

$$\left(\frac{\Delta T}{T}\right)^2_{rms} = \frac{1}{4\pi} \sum_{l=2}^{\infty} (2l+1)\, C_l \exp\left(-\frac{l^2\theta_c^2}{2}\right) \qquad (21)$$

$$\left(\frac{\Delta T}{T}\right)^2_{Q} = \frac{5}{4\pi} C_2 \exp(-2\theta_c^2), \qquad (22)$$

where

$$\langle |a_{lm}|^2 \rangle = C_l = \frac{H_0^4}{2\pi} \int_0^\infty dk \frac{|\delta_k|^2}{k^2} |j_l(k\eta)|^2. \qquad (23)$$

Here j_l is the spherical Bessel function of order l and $\eta = 2H_0^{-1} \equiv 2R_H \simeq 6000\,h^{-1}$ Mpc.

The quantity θ_c can be determined from the response function of the detector, which is usually quoted in terms of a quantity called 'full-width-at-half-maximum', θ_{FWHM}. Usually, $\theta_c \cong 0.425\,\theta_{FWHM}$. The COBE instruments have $\theta_{FWHM} \simeq 7°$ and are designed to detect the large angle anisotropies in the MBR.

Since COBE is essentially probing large angular scales, it is legitimate to use the asymptotic form $P(k) \simeq Ak$ in computing C_l. Then we find that $C_2 = AH_0^4/24\pi$ and $C_l = [6C_2/l(l+1)]$. Substituting these relations into equations (21) and (22) we get $(\Delta T/T)^2_Q = (5.28 \times 10^{-3})(AH_0^4)$ and $(\Delta T/T)^2 = 0.03\,(AH_0^4)$. The quantity (AH_0^4) is directly related to the fluctuations in the gravitational potential $\Phi^2 = (k^3|\phi_k|^2/2\pi^2)$ at large scales. Since $\phi_k = (4\pi G\rho_b)\,(\delta_k/k^2) = (3/2)H^2\,(\delta_k/k^2)$ we find that $AH_0^4 = (8\pi^2/9)\Phi^2$ and we can reexpress the anisotropies as,

$$\left(\frac{\Delta T}{T}\right)_Q \cong 0.22\,\Phi; \left(\frac{\Delta T}{T}\right)_{rms} \cong 0.51\,\Phi. \qquad (24)$$

We can now compare the theoretical results with the COBE observations. To begin with, notice that $(\Delta T_{rms}/\Delta T_Q) \cong 2.3$ if the spectrum has $n=1$. The COBE results allow this ratio to fall between 1.43 and 3.94 with a mean value of 2.29. This is quite consistent with the assumption of $n=1$. (It turns out that a least square fit to the COBE data gives $n=1.1\pm0.5$. We shall, hereafter, assume that $P(k) \propto k$ for small k.

The parameter Φ and the amplitude A can now be determined by comparing equation (24) with COBE result. Within the error bars, we get $\Phi \cong 2.2\times10^{-5}$ and $A=(24\,h^{-1}\ \text{Mpc})^4$. Also note that the quadrupole result gives $C_2^{1/2}=(4\pi/5)^{1/2}\ (\Delta T/T)_Q=(0.76\pm0.24)\times10^{-5}$; thus the maximum permitted value for $C_2^{1/2}$ is about 10^{-5}.

These results impose rather stringent conditions on the models for structure formation. Consider, for example, pure HDM models with a power spectrum of the form discussed in section 2.3. For this spectrum, the density contrast, $\Delta_k=[k^3P(k)/2\pi^2]^{1/2}$ reaches maximum at $k_m=0.69\,k_{FS}$. The maximum value is $\Delta_{max}=[k_m^3P(k_m)/2\pi^2]^{1/2}=7.3\times10^{-4}\ (A/1\ \text{Mpc}^4)^{1/2}\ (m/30\ \text{eV})^2$. Using the COBE result, $A\simeq(24\,h^{-1})^4\ \text{Mpc}^4$ we get $\Delta_{max}\cong 0.42\,h^{-2}\ (m/30\ \text{eV})$ This value is far too small to produce any nonlinear structures by today. We saw earlier that for a mass scale to go nonlinear at a redshift z_{coll}, the density contrast should be about $\delta_0\cong f(1+z_{coll})$ with $f\simeq1.5-2$. Even with $h=0.5$, equation (3) gives only $z_{coll}\simeq0$; that is, structures are beginning to go nonlinear only at the present epoch. Thus COBE bounds rule out pure HDM scenarios.

The COBE constraints on CDM models are somewhat more complicated. We saw earlier that if the CDM spectrum is normalized to give $\sigma(8\,h^{-1}\ \text{Mpc})=(1/b)$ then we get $\sigma(50\,h^{-1}\ \text{Mpc})\simeq(0.1/b)$ which is a factor $2b$ lower than the results of galaxy surveys. The $(\Delta T/T)$ computed from such a model will be a factor $1.2\,b$ lower than the COBE result. Such a normalization will also give unacceptable correlation function unless $b\simeq2$.

On the other hand, if we normalize the CDM spectrum using the COBE results, we will get a larger amplitude of $A_0=5.3\times10^6$. This will make $\sigma_{DM}(8\,h^{-1}\ \text{Mpc})$ overshoot the value of unity. What is more, the shape of the spectrum will be highly curved in the range of $(2\text{-}20)\,h^{-1}$ Mpc. Nonlinear effects could steepen the small scale spectrum, thereby reducing the curvature; but this will also *increase* the amplitude to still higher values.

COBE results, based on Sachs–Wolfe effect, probe the dominant source of gravity, viz. the dark matter. In that sense, dark matter spectrum at large scales *must* be normalized using COBE. This gives $\sigma_{DM}(R)\simeq(R_0/R)^2$ at large R with $R_0\simeq24\,h^{-1}$ Mpc. But the relation between $\sigma_{gal}(R)$ and the underlying dark matter distribution $\sigma_{DM}(R)$ is far from clear. Galaxy surveys do show that $\sigma_{gal}(50\,h^{-1}\ \text{Mpc})\simeq0.2$; since COBE normalization of CDM spectrum also gives $\sigma_{CDM}(50\,h^{-1}\ \text{Mpc})\simeq(24/50)^2\simeq0.2$, it appears that the bias factor $b\simeq1$ at least for $R\gtrsim50\,h^{-1}$ Mpc. This, however, demands that $b<1$ at $r\simeq8\,h^{-1}$ Mpc to reproduce small scale galaxy distribution, unless the shape of the spectrum is very different from that of CDM.

4. Comparison and conclusions

The various observational constraints discussed so far are summarized in Figure 4. The lower bound marked 'high-z objects' arises from demanding that mass scales in the range 10^{11}–$10^{12}\,M_\odot$ should go nonlinear by $z=4.5$. The bound marked 'large scale streaming' comes from the reconstruction of velocity fields[38]. At large scales, we have marked the $\sigma(R)$ arising from the COBE results.

To quantify the nature of these constraints we have fitted (see Figure 5) a series of model spectra to the data. These spectra have the form:

$$P(k)=\frac{Ak}{1+(k/k_c)^n}. \tag{25}$$

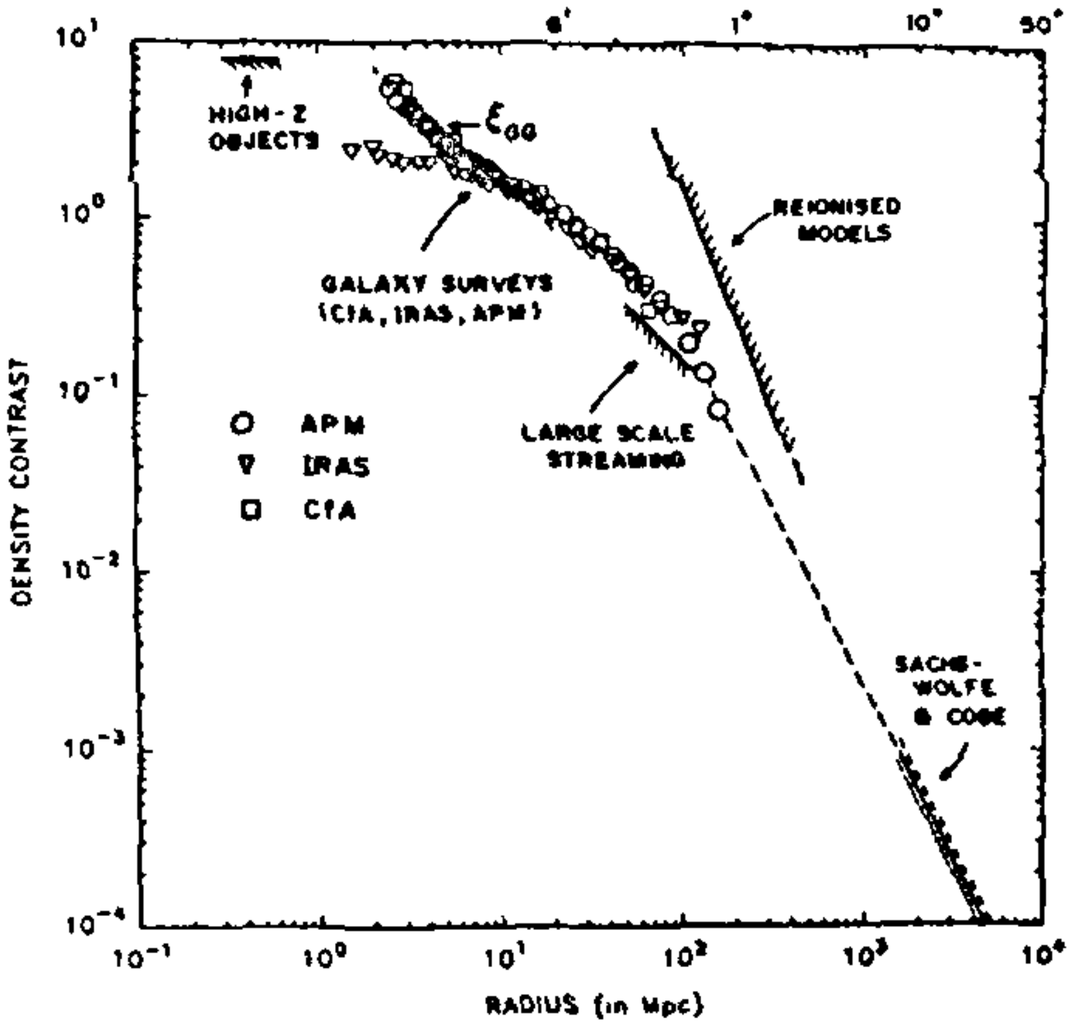

Figure 4. Various constraints on the rms fluctuations in mass, $\sigma(R)=\langle(\delta M/M)_R^2\rangle^{1/2}$, are plotted against the scale R. Within a factor or order unity, this $\sigma^2(R)$ also represents the power in each octave, $[k^3P(k)/2\pi^2]$, at $k=R^{-1}$. At the right-bottom, the result from COBE based on $(\Delta T/T)_{rms}$ is marked assuming a spectrum which is scale-invariant at large scales. The $\sigma(R)$ determined from CfA, IRAS and APM surveys are shown by different symbols. In the case of APM, $W(\theta)$ was inverted to give $\xi(r)$. We have not included QDOT data in this figure because it is based on cubical cells. The lower bound on $\sigma(R)$—marked 'high-z objects'—arises from requiring that mass scales in the range $(10^{10}$–$10^{11})\,M_\odot$ should go nonlinear by $z=4.5$. The bound marked 'large scale streaming' arises from the POTENT reconstruction of velocity fields. We have also shown the (rather weak) upperbound from small angle anisotropies in MBR in the reionized models and the slope of the galaxy–galaxy correlation function ($h=0.5$).

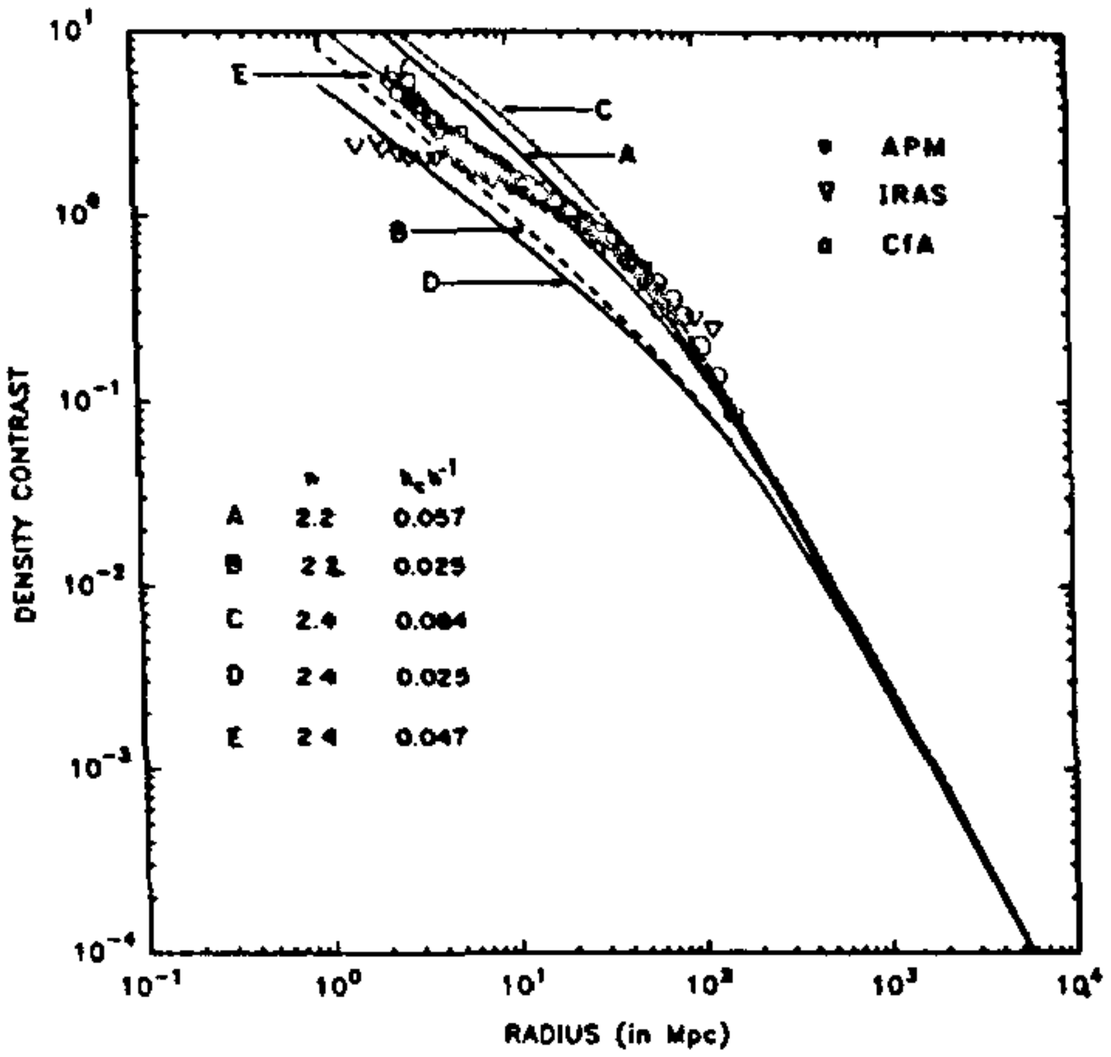

Figure 5. The results of galaxy surveys and COBE anisotropy are fitted using simple test spectra of the form $P(k)=Ak[1+(k/k_c)^n]^{-1}$. All the spectra are normalized using the maximum permitted value of a_2 from COBE, viz. $a_2=10^{-5}$. There is reasonable agreement for $n=2.4$, $k_c=0.047\,h$ (the fit can be marginally improved by choosing $n=2.41$ and $k_c=0.047\,h$). This suggests a length scale of $k_c^{-1}=21\,h^{-1}$ Mpc in the theory. We have set $h=0.5$.

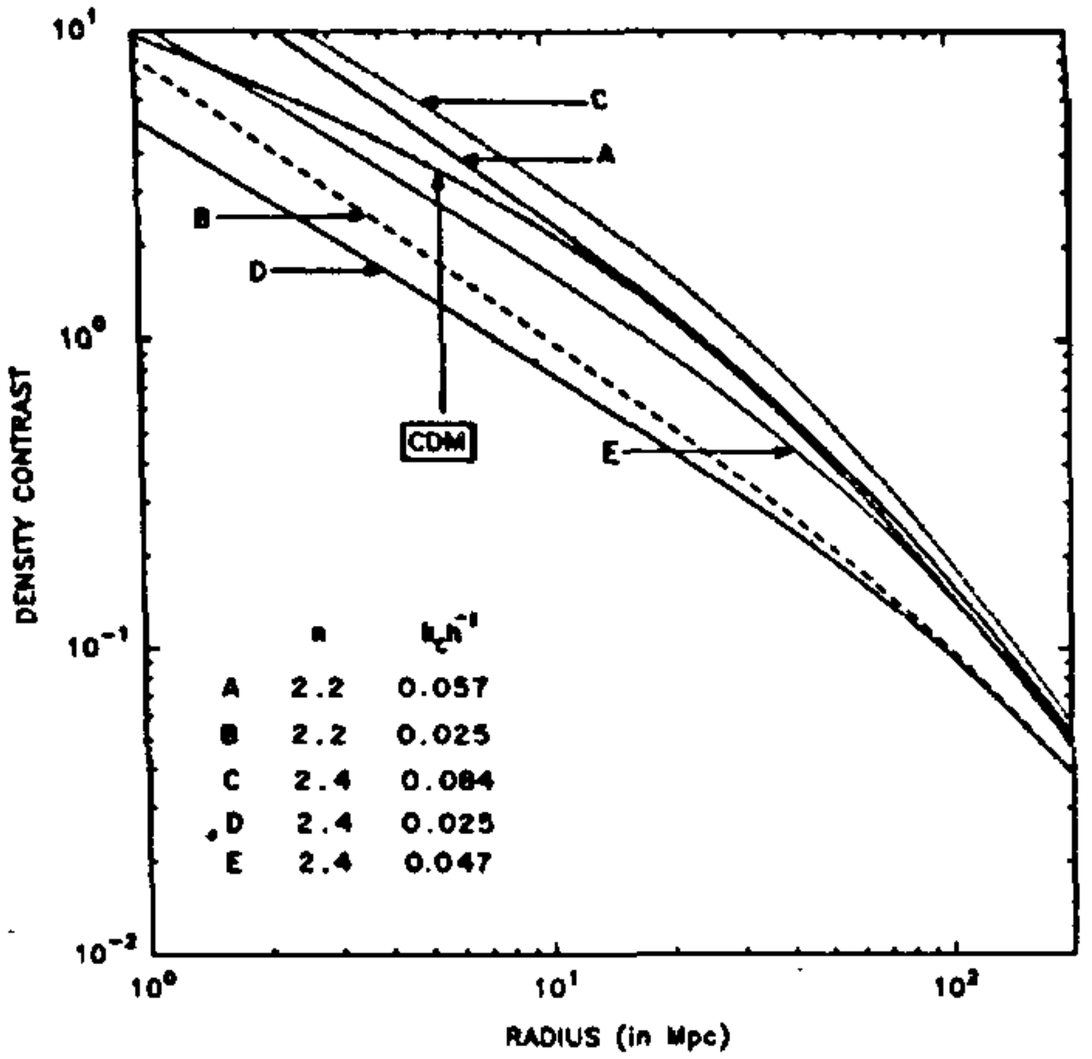

Figure 6. The model spectra in Figure 4 are shown in an enlarged scale and compared with CDM (dash-dot-dot curve). All curves are normalized by COBE result. Note that CDM spectra show much more significant curvature compared to the model spectra.

The amplitude A is fixed using the COBE result of $(C_2)_{max}=10^{-5}$. That leaves two free parameters: (i) an index n which determines the slope of the spectra at large k and (ii) a length scale k_c^{-1} which fixes the location at which the spectrum bends. The density contrast $\sigma(R)=\langle(\delta M/M)_R^2\rangle^{1/2}$ calculated from equation (25) is plotted for five different values in Figure 5. Also plotted in the same figure are the $\sigma(R)$ determined from a few galaxy surveys[2]. A good fit is achieved for $n=2.4$, $k_c=0.047\,h$ Mpc^{-1} (curve E). We have also shown two curves ($n=2.2$, $k_c=0.057\ h$ Mpc^{-1} and $n=2.4$, $k_c=0.084\ h$ Mpc^{-1}) which overshoots the data and two curves ($n=2.2$, $k_c=0.025\,h$ Mpc^{-1} and $n=2.4$, $k_c=0.025\,h$ Mpc^{-1}) which undershoots the data. These fits suggest that a sharply bending power spectrum with a length scale of about $L\simeq k_c^{-1}\simeq 21\,h^{-1}$ Mpc may be required to explain all the observations. Notice that these spectra are characterized by pure power law forms for large and small k. In contrast, a CDM spectrum *with the same COBE normalization* shows much more curvature. We have shown in Figure 6 such a CDM spectrum along with the curves A–E. The CDM spectrum agrees fairly well with the best fit curve at large scales but has a very different shape at small scales. It should be clear that the major trouble is not so much as the amplitude of the spectrum as its shape.

In summary, we may say that all simple models of galaxy formation have some difficulty in explaining the observational data. It is possible to produce models which will explain all the data provided we have more free parameters in the theory. All such possibilities essentially revolve around using two different kinds of contributions to Ω in a judicious way. For example, models containing both cold and hot dark matter or CDM models with $\Omega_{vac}\neq 0$ can be made to work. All these models, unfortunately, suffer from unaesthetic fine tuning of parameters.

Alternatively, these difficulties may dissappear when the nonlinear evolution of density inhomogeneities is understood better. In particular, it is important to investigate both the steepening of $\sigma(R)$ in the nonlinear regime as well as the dependence of the bias factor b on the scale R. If dynamical processes can give $b<1$ at small scales and steepen the spectrum properly, pure CDM or a variant of it can be a viable model.

Note added in proof: The following two are among many preprints which have appeared in recent months analysing COBE results: (1) There is a preprint by A. Gould (IASSNS–AST-92/29) suggesting that the quadrupole anisotropy in the COBE data is consistent with zero at 13 per cent confidence level. (2) A. R. Liddle and D. H. Lyth (LANC-TH 8-92) have analysed extensively several models for which the initial spectrum is *not* scale-invariant. It turns out that COBE imposes severe constraints on these models as well.

1. Peebles, P. J. E., *The Large-scale Structure of the Universe*, Princeton University, Princeton, 1980; Padmanabhan, T., *Structure Formation in the Universe*, Cambridge University Press, Cambridge, 1992. (in press)
2. Padmanabhan, T. and Subramanian, K., *Bull. Astron. Soc. India*, 1992, **20**, 1
3. See for eg., Carney, B. W. and Latham, D. W., in *Dark Matter in the Universe* (eds. Kormendy, J. and Knapp, G. R.), IAU Symposium 117, Reidel, Dordrecht, 1987, p. 39; Tremaine, S. and Lee, H. M., in *Dark Matter in the Universe*, Word Scientific, Singapore, 1987, p. 103, Rubin, V. C., in *After the First Three Minutes* (eds. Holt, S. S., Bennett, C. L. and Trimble, V.), AIP, New York, 1991.
4. Observational status of the primordial nucleosynthesis is reviewed, for example, Pagel, B. E. J., *Phys. Scr.*, 1991, **T36**, 7.
5. Bardeen, J., Steinhardt, P. and Turner, M. S., *Phys. Rev.*, 1983, **D28**, 679. Guth, A. and Pi, S. Y., *Phys. Rev. Lett.*, 1982, **49**, 1110, Hawking, S. W., *Phys. Letts.*, 1982, **B115**, 295; Starobinsky, A. A., *Phys. Lett.*, 1982, **B117**, 175, Padmanabhan, T., Seshadri, T. R. and Singh, T. P., *Phys. Rev.*, 1989, **D39**, 2100 For a review, see Brandenberger, R. H., *Rev. Mod. Phys.*, 1985, **57**, 1; Narlikar, J. V. and Padmanabhan, T., *Annu. Rev. Astron. Astrophys.*, 1991, **29**, 325.
6. See for eg. Gibbons, G. W., Hawking, S. W. and Vachaspati, T., *The Formation and Evolution of Cosmic Strings*, Cambridge University Press, 1990; Turok, N., *Phys. Scr.*, 1991, **T36**, 135 and references cited therein.
7. Harrison, E. R., *Phys. Rev.*, 1970, **D1**, 2726, Zeldovich, Ya. B., *Mon. Not. R. Astron. Soc.*, 1972, **160**, 1p.
8. These topics have been discussed by several authors. A sample of reference will be: Zeldovich, Ya. B., *Zh. Eksp. Teor. Fiz.*, 1965, **48**, 986; Lee, B. W. and Weinberg, S., *Phys. Rev. Lett.*, 1977, **39**, 165; Cowsik, R. and McClelland, J., *Phys. Rev. Lett.*, 1972, **29**, 669; Gerstein, G. and Zeldovich, Ya. B., *Zh. Eksp. Teor. Fiz. Pisma Red.*, 1966, **4**, 174; also see the review: Dolgov, A. and Zeldovich, Ya B., *Rev. Mod. Phys.*, 1981, **53**, 1.
9. For a general overview, see eg. Gelmini, G., in *Dark Matter in the Universe* (eds. Galeotti, P. and Schramm, D. N.), Kluwer, Denmark, 1990, p. 25; Caldwell, D. O., VCSB-HEP preprint 91-04, 1991; Ellis, J., *Phys. Scr.*, 1991, **T36**, 142; for a review of laboratory searches of axions, see eg., Kim, J. E., *Phys. Rep.*, 1987, **150**, 1.
10. Bond, J. R. and Szalay, A. S., *Astrophys. J.*, 1983, **276**, 443
11. Peebles, P. J. E., *Astrophys. J.*, 1983, **263**, L1; Davis, M. *et al.*, *Astrophys. J.*, 1985, **292**, 371.
12. See eg., Efstathiou, G., in *Physics of the Early Universe* (eds. Peacock, J. A., Heavens, A. F. and Davies, A. T.), Proceedings of the 36th Scottish Universities Summer School in Physics, Adam Hilger, 1990, p. 361, Peacock, J. A., *Statistics of Cosmological Density Fields*, Edinburgh Astronomy Preprint, 1991, No. 22/91.
13. Meszaros, P., *Astron. Astrophys.*, 1975, **38**, 5.
14. A sample of references will be: Davis, M. *et al.*, *Astrophys. J.*, 1985, **292**, 377; Frenk, C. S. *et al.*, *Nature*, 1985, **317**, 595, Frenk, C. S. *et al.*, *Astrophys. J.*, 1988, **327**, 507, White, S. D. M. *et al.*, *Nature*, 1987, **330**, 451; White, S. D. M. *et al.*, *Astrophys. J.*, 1987, **313**, 505; Centrella, J. and Mellott, A., *Nature*, 1982, **305**, 196; White, S. D. M., Frenk, C. S. and Davis, M., *Astrophys. J.*, 1983, **274**, L1.
15. Padmanabhan, T. and Nityananda, R., 1992, unpublished.
16. The 'universal' behaviour of h is implicit in the simulation results of Efstathiou, G. *et al.*, *Mon. Not. R. Astron. Soc.*, 1988, **235**, 715. It has been explicitly noted in Hamilton *et al*, see ref. 17.
17. Hamilton, A. J. S. *et al.*, *Astrophys. J.*, 1991, **374**, L1–L4.
18. Padmanabhan, T. and Subramanian, K., TIFR-TAP-2/92 preprint, submitted for publication, 1992.
19. Davis, M. and Peebles, P. J. E., *Astrophys. J.*, 1983, **267**, 465; Rowan-Robinson, M., *et al.*, *Mon. Not. R. Astron. Soc.*, 1990, **247**, 1; Efstathiou, G. *et al.*, *Mon. Not. R. Astron. Soc.*, 1990, **247**, 10p. Saunders, W. *et al.*, *Nature*, 1991, **349**, 32.
20. The CfA, IRAS and APM data are adapted from Hamilton, A. J. S. *et al.*, *Astrophys. J.*, 1991, **374**, L1. The original data are based on Huchra J. *et al.*, *Astrophys. J. Suppl.*, 1983, **52**, 89; Maddox, S. *et al.*, *Mon. Not. R. Astron. Soc.*, 1990, **242**, 43p; **243**, 692; Strauss, M. A. *et al.*, *Astrophys. J.*, 1990, **361**, 49. The DOT data were kindly provided by M. Rowan-Robinson and are based on Saunders, W. *et al.*, 1992, Oxford Astrophysics preprint, ref. no. OUAST/92/4 (to be published in *MNRAS*), 1992.
21. For a discussion and examples of 'biasing', see Rees, M. J., *Mon. Not. R. Astron. Soc.*, 1985, **213**, 75p; Dekel, A. and Silk, J., *Astrophys. J.*, 1986, **303**, 39; Silk, J., *Astrophys. J.*, 1985, **297**, 1
22. Carlberg, R. G., Couchman, H. M. P. and Thomas, P. A., *Astrophys. J.*, 1990, **352**, L29; Evrad, A., *Astrophys. J.*, 1986, **310**, 1; West, M. J. and Richstone, D. O., *Astrophys. J.*, 1988, **335**, 532.
23. Centralla, J. and Mellot, A., *Nature*, 1982, **305**, 196; White, S. D. M., Frenk, C. S. and Davis, M., *Astrophys. J.*, 1983, **274**, L1, White, S. D. M., in *Inner Space/Outer Space* (eds. Kolb, E. W. *et al.*), Chicago University Press, Chicago, 1986, p. 228.
24. Davis, M. *et al.*, *Astrophys. J.*, 1985, **292**, 371; Frenk, C. S. *et al.*, *Nature*, 1987, bf 317, 595; Frenk, C. S. *et al. Astrophys. J.*, 1988, **327**, 507; White, S. D. M. *et al.*, *Nature*, 1987, **330**, 451; White, S. D. M. *et al.*, *Astrophys. J.*, 1987, **313**, 505.
25. Maddox, S. J. *et al.*, *Mon. Not. R. Astron. Soc.*, 1990, **242**, 43p; Saunders, W. *et al.*, *Nature*, 1991, **349**, 32.
26. Tyson, J. A., *Astron. J.*, 1988, **96**, 1; Cowie, L. L. *et al.*, *Astrophys. J. Lett*, 1990, **360**, L1; Cowie, L. L., *Phys. Scr.*, 1991, **36**, 102 and the references cited therein; Koo, D., in *Evolution of the Universe of Galaxies* (ed. Kron, R. G.), A.S.P. Conference Series, 1990, vol. 10, p. 268.
27. For a discussion of various aspects of this problem, see *Evolution of Universe of Galaxies* (ed. Kron, R. G.), ASP, 1990, vol. 10, 1990.
28. Schneider, D. P., Schmidt, M. and Gunn, J. E., *Astrophys. J.*, 1992, (in press)
29. Kashlinsky, A. and Jones, J. T., *Nature*, 1991, **349**, 753; Turner, E. L., *Astron. J.*, 1991, **101**, 5.
30. Rees, M. J., *Mon., Not. R. Astron. Soc.*, 1986, **218**, 25; *QSO Absorption Lines* (eds. Blades, J. C., Turnshek, D. and Norman, C. A.), Cambridge University Press, Cambridge; Carswell, R. F., in *The Epoch of Galaxy Formation* (eds. Frenk, C. S., Ellis, R. S., Shanks, T., Heavens, A. F. and Peacock, J. A.), Kluwer, Dordrecht, 1989; Hunstead, R. W. *et al.*, *Astrophys. J.*, 1988, **329**, 527; Bechtold, J., in *High Redshift and Primeval Galaxies* (eds. Bergeron, J., Kunth, D., Rocca-Volmerange, B. and Tran Tranh Van, J.), Frontiers, Paris, 1987, p. 397; Turner, E. L. and Ikeuchi, S., *Astrophys. J.*, 1992, **389**, 478.
31. Gunn, J. E. and Peterson, B. A., *Astrophys. J.*, 1965, **142**, 1633; Steidel, C. C. and Sargeant, W. L. W., *Astrophys. J. Letts.*, 1987, **318**, L11; Also see Schneider *et al.*, *Astron. J.*, 1989, **98**, 1951.
32. See eg. Shapiro, P. R. and Giroux, M. L., *Astrophys. J. Letts.*, 1987, **321**, L107; Shapiro, P. R. and Giroux, M. L., in *The Epoch of Galaxy Formation* (eds. Frenk, C. S., Ellis, R. S., Shanks, T., Heavens, A. F. and Peacock, J. A.), Kluwer, Dordrecht, 1989, 153p; Shapiro, P. R., Giroux, M. L. and Babul, A., in *After the First Three Minutes* (eds. Holt, S. S., Bennett, C. L. and Trimble, V.), AIP, New York, 1991; Couchman, H. P. M. and Rees, M. J., *Mon. Not. R. Astron. Soc.*, 1986, **221**, 1513.
33. Lilly, S. J., in *The Epoch of Galaxy Formation* (eds. Frenk, C. S., Ellis, R. S., Shanks, T., Heavens, A. F. and Peacock, J. A.), Kluwer, Dordrecht, 1989, 163; Lilly, S. J., *Astrophys. J.*, 1989, **340**, 77.
34. Uson, J. M., Bagri, D. S. and Cornwell, T. J., *Phys. Rev. Lett*, 1991, **67**, 3328
35. Subramanian, K. and Swarup, G., *A cluster of HI Rich Protogalaxies at Redshift $z \approx 3.4$?*, submitted to *Nature*, 1991.

36. Yahil, A., Tammann, G. and Sandage, A., *Astrophys. J.*, 1977, **217**, 903; For a review of different measurements, see: Lynden-Bell, D. and Lahav, O., in *Large Scale Motions in the Universe* (eds. Rubin, V. C. and Coyne, G.), Princeton University Press, Princeton, 1989.
37. Dressler, A., *Astrophys. J.*, 1987, **317**, 1; Lilje, P. B., Yahil, A. and Jones, B. J. T., *Astrophys. J.*, 1986, **307**, 91; Lynden-Bell, D. *et al.*, *Astrophys. J.*, 1988, **326**, 16; Burnstein, D. *et al.*, *Galaxy Distances and Deviations from Universal Expansions* (eds. Madore, B. F. and Tully, R. B.), Reidel, Boston, 1986, p. 123; For a detailed review, see Burstein, D., *Rep. Prog. Phys.*, 1990, **53**, 421.
38. Bertschinger, E. and Dekel, A., *Astrophys. J.*, 1989, **336**, L5; Dekel, A., Bertschinger, E. and Faber, S. M., *Astrophys. J.*, 1990, **364**, 349; Bertschinger, E. *et al.*, *Astrophys. J.*, 1990, **364**, 370.
39. See the contributions by Strauss, M., Davis, M. and Yahil, A., in *Large Scale Motions in the Universe* (eds. Ruben, V. C. and Coyne, G.), Princeton University Press, Princeton, 1988, p. 255; Strauss, M. and Davis, M., in *The Large Scale Structure of the Universe* (ed. Audouze, J.), IAU Symposium 130, 1988; Rowan-Robinson, M. *et al.*, *Mon. Not. R. Astron. Soc.*, 1990, **247**, 1; Efstathiou, G. et al., Mon. Not. R. Astron. Soc., 1990, **247**, 10p; Saunders, W. *et al.*, *Nature*, 1991, **349**, 32.
40. Bond, J. R., in *The Early Universe* (eds. Unruh, W. G. and Semenoff, G. W.), Reidel, Dordrecht, 1988; and in *Large Scale Structures of the Universe* (eds. Audouze, J., Pelletar, M. C. and Szaiay, H), IAU Symposium 130, Kluwer, Dordrecht, 1988.
41. Jones, B. J. T. and Wyse, R. F. G., *Astron. Astrophys.*, 1985, **149**, 144.
42. Bond, J. R. and Efstathiou, G., *Astrophys. J.*, 1984, **285**, L45.
43. Smoot, G. F. *et al.*, 1992, preprint.
44. Padmanabhan, T. and Narasimha, D., preprint TIFR-TAP-3/92, 1992; Wright, E. L. *et al.*, preprint, 1992.
45. Peebles, P. J. E., *Astrophys., J. Lett.*, 1982, **263**, L1.

ACKNOWLEDGEMENTS. I thank D. Narasimha, R. Nityananda and K. Subramanian for useful discussions and comments and M. Rowan Robinson for his kind permission to use the QDOT data.

RESEARCH COMMUNICATIONS

Snow line depression over Tibet during last Ice Age

S. K. Gupta and P. Sharma
Physical Research Laboratory, Ahmedabad 380 009, India

The Tibetan plateau has received considerable attention in recent years for its role in influencing the regional and global climatic changes during the last Ice Age. However, debate persists on the thickness and areal extent of the ice cover for which estimates of the past positions of the snowline are required. Based on qualitative interpretation of geological deposits, varying estimates (200–1500 m) of the snowline depression during the last Ice Age have been proposed. We estimate this parameter to be in the range 700–850 m (maximum 1000–1170 m) from the translation of $\delta^{18}O$ data to temperature lowering on the Dunde ice cap in Tibet. Such a lowering of the regional snow line would have resulted in an extensive but marginally thick ice sheet sensitive to small regional temperature fluctuations as revealed by the isotope record of the Dunde ice cores and the palaeovegetation record of Tsokar lake in Ladakh. In this study, we have not considered the effect of possible precipitation reduction, which is likely to further reduce estimates of snow line depression.

THE Tibetan plateau, with an area of nearly 2×10^6 km^2 at an average altitude of over 5000 m above sea level, exerts significant control on the Asian monsoon circulation pattern[1–5]. During the last Ice Age, also known as the last glacial stage (LGS), summer monsoon circulation is supposed to have been weak or absent[3,6,7] and the climate of Tibet was probably drier than today. Considerable debate persists as to whether the plateau was covered by an extensive[8–10] or a marginal[11–14] ice sheet. Estimates of the thickness and the extent of glaciation in Tibet during LGS are important because of its possible implications in palaeoclimatic modelling involving presence or absence of snow cover over Tibet as an important boundary condition.

A kilometre thick and extensive ice sheet as envisaged by Kuhle *et al.*[8] would amount to an additional ice volume of about 3×10^6 km^3 at the last glacial maximum (LGM), about 18 kyr ago. This would correspond to an equivalent global sea level change of approximately 7–8 m. The contribution of such an ice sheet to the $\delta^{18}O$ of the ocean water can be larger than suggested just by the hypothesized volume of this ice sheet due to introduction of nonlinearity between the $\delta^{18}O$ and the global ice volume[15]. This effect arises due to the fact that the ice sheet on Tibetan plateau would grow mainly by increase in the ice thickness, thus raising the altitude of precipitation. This would induce a strong change in the mean $\delta^{18}O$ of the ice during ice sheet build-up (the altitude effect). A relatively thin ice cover over Tibet would not significantly alter the estimate of global ice volume and the oceanic $\delta^{18}O$ record.

The difference between a thick versus thin ice sheet may also manifest in its response to a small warming event. In the case of a thick (~1 km) ice sheet over Tibet, a small warming event would not be able to lower the snowline (or the equilibrium line altitude, ELA) below the top of the ice surface and may therefore not result in significant melting of the ice mass. In contrast, small temperature-induced movements of ELA would sensitively affect the melting of a thin (~200 m) Tibetan ice sheet.

Kuhle has repeatedly argued[8–10] that a large ice sheet existed on the Tibetan plateau during the late